# EXPERIMENTAL INVESTIGATION OF ULTRAHIGH VACUUM ADHESION AS RELATED TO THE LUNAR SURFACE



ELEVENTH QUARTERLY PROGRESS REPORT

1 JANUARY THROUGH 31 MARCH 1967

J. A. Ryan
Principal Investigator
R&D/Lunar and Planetary
Sciences Branch

Prepared for:
NASA/Office of Advanced
Research and Technology
Washington, D.C.

Contract NAS 7-307

Date of Issue:
26 June 1964
A-830-BBK3-37



MISSILE AND SPACE SYSTEMS DIVISION
DOUGLAS AIRCRAFT COMPANY, INC.
SANTA MONICA, CALIFORNIA

TABLE OF CONTENTS

ABSTRACT

Work during this quarter has consisted of 1) completion of the system modifications and repairs initiated during the previous quarter, 2) measuring the adhesion between differing silicate minerals whose contact faces have been formed "simultaneously" by cleavage at ultrahigh vacuum, and 3) continuation of the theoretical analyses of the observed long-range attractive forces.

The system modifications consisted of the design and air testing of a double cleavage device and an electrometer probe, and the installation of additional ports and feedthrus to permit operation of these, and a residual gas analyzer which is to be included in the system. System repairs involved removing leaks that developed during the previous quarter. These modifications and repairs were completed by the early part of February.

Eight double cleavage runs were made during the remainder of the quarter. Of these one was successful, one, though basically unsuccessful, provided some interesting information, and the remaining six were failures. The difficulties encountered appear to have been largely overcome and it is expected that a considerable increase in success percentage will occur during the next quarter.

The successful double cleavage run was for orthoclase (001) and microcline (001). The adhesion force between these was about 0.4 gm initially, and the adhesion gradually dropped below detectable in a few hours. A long range attractive force was present, but this had no tendency to rotate or

displace the samples; also there was no attraction to adjacent metal. No repulsion was evident at any time. The basically unsuccessful run, which provided some information, was also for orthoclase (001) and microcline (001). For this run, both samples broke into several pieces. However, a small segment of the microcline (upper sample) remained in place and several fragments of the bottom sample attached themselves to it indicating the presence of a long range attractive force. These fragments remained attached until shortly after the system was returned to atmospheric pressure.

Due to the design problems encountered in the double cleavage, we have not as yet placed the electrometer probe and residual gas analyzer in the system. It is expected that this will be done during the next quarter. In the interim, we have placed the analyzer in a second, similar, ultrahigh vacuum system. No results are available from this system as yet. The readout instrumentation for the load cells, ordered at the beginning of the previous quarter, though past due, has not as yet been received.

Theoretical studies of the cause of the long range attractive force have continued. Results to date will be presented at the "Adhesion of Materials In Space Environments" symposium, Toronto, Canada, May 1-2, 1967. The paper is reproduced in Appendix A.

The recent vacuum cleavage data and their implications to the moon will also be presented at the symposium and this paper is reproduced in Appendix B.

## 1.0 INTRODUCTION

### 1.1 General

This report presents a summary of work accomplished during the period January 1, 1967, through March 31, 1967, on the study of the ultrahigh vacuum frictional-adhesional behavior of silicates as related to the lunar surface. This work is being conducted for the Office of Advanced Research and Technology, National Aeronautics and Space Administration, under Contract NAS 7-307.

### 1.2 Purpose and Importance of the Program

The primary purpose of the program is to obtain quantitative experimental data concerning the ultrahigh vacuum adhesional behavior of the materials which may presently exist at the lunar surface and to obtain similar data for adhesion between these lunar surface materials and those engineering materials which may be placed upon the surface. Additional purposes of this program are to analyze the data with regard to the possible reactions of granular materials to engineering operations and to investigate means by which any problems posed by these reactions may be minimized.

The importance of this program is that adhesion phenomena can pose serious problems to lunar surface operations.

### 1.3 Work Accomplished During This Quarter

The first month of the quarter consisted of modifying and repairing the experimental chamber, air testing the double cleavage device, and continuing

the theoretical studies of the cause(s) of the long range attractive forces observed after vacuum cleavage. The remaining two months of the quarter consisted of double cleavage ultrahigh vacuum runs, the initiation of studies of the source(s) of the gas bursts observed during cleavage operations, and continued theoretical studies.

## 2.0 INSTRUMENTATION

The following sections describe the major system modifications made or begun during this quarter.

### 2.1 Load Cell

A load cell was constructed during the previous quarter. The purposes of the cell are to apply load force to the samples after cleavage and to measure the force-distance relationship of the long range attractive force. The required readout instrumentation was ordered at the beginning of the quarter. The original due date has long since passed, but the equipment has not arrived and the best available information is that we can expect it sometime during April. Because of this difficulty, the mechanical spring is still being used to measure adhesion force.

### 2.2 Chamber Modification and Repair

The chamber was modified by the addition of two ports and two electrical feedthrus to allow an electrometer probe and a residual gas analyzer to be placed in the system. Concurrently, we repaired various leaks which had developed during the latter part of the previous quarter.

2.2.1 Electrometer Probe: The purpose of the electrometer probe is to measure the charge distribution over the surfaces of the vacuum cleaved samples. The probe design was discussed briefly in the previous quarterly report. Construction has been completed during this quarter.

The probe has not as yet been mounted into the system due to the difficulties encountered in obtaining successful double cleavage runs. It is however planned to use the probe during the next quarter since the major difficulties involved in obtaining double cleavage appear to have been resolved.

2.2.2 Residual Gas Analyzer: Gas bursts have been noted during most vacuum cleavages. These are not associated with the samples, see previous quarterly reports, but rather appear to be the result of the vibrations produced during the cleavage operations. There are three likely effects which could produce gas bursts as a result of system vibration. These are a) desorption of physically adsorbed material from the chamber walls, b) the momentary opening of microcracks in the chamber walls, and c) desorption of gases from the ion pump (such as helium) which are poorly pumped and held.

An additional port was added to the chamber to permit inclusion of a CEC Residual Gas Analyzer.

2.3 Double Cleavage Device

The purpose of this device is to obtain two simultaneous cleavages, in ultra-high vacuum, of differing silicate minerals and then to permit measurement of the adhesion between these unlike samples.

The initial design of this device was similar to that of the single cleavage device, the single chisel point simply being replaced by two points and the anvil being modified to supply support opposite both cleavage points. The procedure was to a) fasten the two samples together by means of a copper cylinder attached to a horizontal spring, b) bring the chisel and anvil into position (the chisel tips being inserted in slots cut into each sample), c) apply a gradually increasing pressure until the cleavages were obtained, d) rely upon the horizontal spring to pull the center pieces out of the way, e) then, remove the chisel and anvil from the sample vicinity, and finally, f) lower the remaining sample halves into contact for the adhesion measurement. This procedure appeared to work well in air, but proved to be quite inadequate at vacuum. The major problem was the wide variations in sample strength which produced difficulties in the maintenance of proper sample position and sample integrity.

Most of the air tests were made with non-silicate samples which did not possess the hardness of the silicates. This was done in order to preserve our limited supply of suitable sample material. However, one air test was made with silicates and was successful. Nevertheless, subsequent events proved that this success was to a large degree fortuitous. The vacuum runs showed that variations in sample strength almost invariably led to one sample cleaving first. Once this occurred one or both of the following would generally occur: The other sample would fracture into a number of pieces; and/or the horizontal spring would tilt the remaining sample parts to the degree that the second cleavage could not be obtained.

The principal modifications made to remove (or reduce) these problems were:

a) Attaching the copper cylinder directly to the anvil and removing the horizontal spring;

b) Changing the anvil shape to provide more positive sample support.

We have made two runs since the incorporation of these modifications, one of which was successful and the other of which was nearly so.

## 3.0 EXPERIMENTAL DATA

Eight ultrahigh vacuum double cleavage runs were made during this quarter. Of these, one was successful and one, though basically unsuccessful, provided interesting qualitative information.

Run #51 Orthoclase (001) and Microcline (001) Double Cleavage

The double cleavage was performed at a system pressure of $2 \times 10^{-10}$ mm Hg. A pressure burst to about $5 \times 10^{-9}$ mm Hg was observed. During cleavage, the upper sample (Microcline) broke not only at the desired spot but also at the cross-pin hole holding it to the mechanical spring. The lower sample broke into a number of pieces. As the upper sample was lowered, several chips of the fractured orthoclase attached themselves to the microcline fracture face. The largest chip was of dimensions about 0.5 x 0.5 x 1.0mm. This attachment demonstrated the existance of adhesion and the indications were that a long range attractive force was present.

We were unable to remove the orthoclase chips from the microcline, but we were able with the chisel to move them over the surface to some degree. The particles remained attached until shortly after the system was brought to

atmospheric pressure. At that time, all indications of adhesion disappeared.

Run #52 Orthoclase (001) and Microcline (001) Double Cleavage

The double cleavage was performed at a system pressure of $2 \times 10^{-10}$ mm Hg. A pressure burst to about $5 \times 10^{-9}$ mm Hg was observed. Both cleavages were good. No realignment of the samples occurred so that all contacts were made with the respective a-axes aligned. First contact was made five minutes after cleavage. This resulted in an adhesion force of about 0.4 gm. This force gradually decreased to below measurement capabilities in about two hours. The data are shown in Figure 1.

A long range attractive force was noted for all measurements. This force, however, did not give any indications of producing sample rotation or displacement. No sample repulsion was present at any time.

## 4.0 DISCUSSION

The limited data obtained to date on the adhesion between dissimilar silicates cleaved in ultrahigh vacuum demonstrate that dissimilar silicates will adhere. The adhesional behavior is similar to that of like vacuum cleaved silicates. Probably the most interesting finding to date is that for both runs the long range force was attractive. Discussions in previous quarterly reports have indicated that, particularly with dissimilar vacuum cleaved surfaces, long range repulsive forces can be produced. Obviously, two runs are not sufficient to exclude this possibility.

In the previous quarterly report, we presented ways in which vacuum cleavage through defect-produced polarization fields could cause electrostatic surface charging. A more detailed discussion including effects of non-uniform

impurity distributions is given in Appendix A.

These effects, for dissimilar vacuum-cleaved minerals placed in contact, can produce both long range attractive and/or repulsive forces. In addition, for dissimilar minerals the respective work functions must be considered. These work function differences, after cleavage has produced nascent surfaces, produce surface polarization and hence, attraction between the surfaces. Further data are required to determine whether the possible repulsion-producing mechanisms can on occasion outweigh the work function effect.

## 5.0 CONCLUSIONS

There are not sufficient data as yet to reach any firm conclusions concerning the adhesional behavior of dissimilar, vacuum cleaved, silicates. However, the findings to date can be summarized as follows:

a) Dissimilar silicates cleaved in ultrahigh vacuum can adhere.

b) The adhesional behavior of these dissimilar silicates is similar to that of like silicates.

c) Though theory predicts that a repulsive force can be present, none has yet been observed.

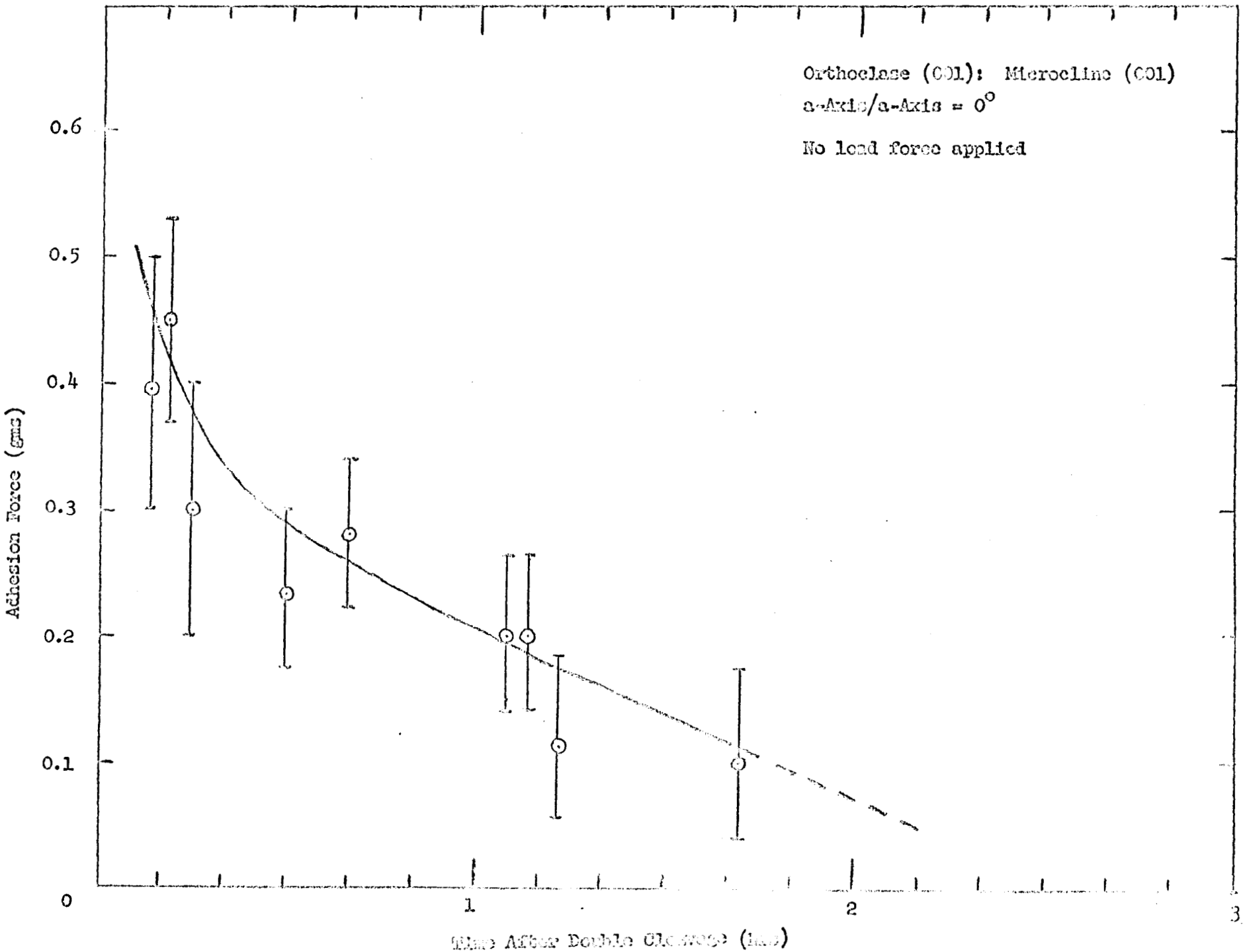
Orthoclase (001): Microcline (001)
a-Axis/a-Axis = 0°
No load force applied
Adhesion Force (gms)
0.6
0.5
0.4
0.3
0.2
0.1
0
1
2
3
Time After Double Cleavage (hrs)

Figure 1

## Appendix A



# Production of Surface Electrostatic Charging on Dielectrics Cleaved in Vacuum: Theoretical

by Jack J. Grossman*

To be presented at Adhesion of Materials in Aerospace Environments Symposium

May 1-2, 1967, Toronto, Canada

ABSTRACT

Ryan (this Conference) has observed the formation of considerable surface charging for silicates cleaved at $10^{-10}$ torr. This charging is stable, apparently non-uniform on a macroscopic scale, persists to $10^{-4}$ torr, and contributes significantly to the adhesion. Additional observations have been that the resultant force field is of such a nature that it can rotate the samples into alignment, and that while on some occasions the samples are attracted to any metal in the vicinity, on other occasions there is no attraction. This paper considers mechanisms which could be responsible for this charging; in particular, the electronic structure of crystalline dislocations and non-uniform impurity distributions which produce charge mosaics.

A number of theoretical models are discussed by which an electric polarization can be induced into non-piezoelectric, dielectric crystals. Then during cleavage through such a polarization field, complementary charge distributions are produced on opposite faces of the cleavage plane.

Pratt and Eshelby, et al., postulated a Debye-Huckel type atmosphere surrounding an edge dislocation. They related crystal fracture strength, in part, to the electrical work required to remove a dislocation from its atmosphere. The electrical effects of dislocation migration in NaCl have been measured since

then by a number of investigators and establish an experimental basis for relating part of the long range electrical forces on cleavage surfaces to the motion of bundles of edge dislocations and the deformation history of the specimen.

Paired cation-anion vacancies and Frenkel defects are examples of more simple defect systems which contribute to electrical charge effects, especially in the presence of non-uniform impurity distributions. Deryagin's and Bryant's observation of charge mosaics in reversible crack propagation is an example of this. Finally, some brief comments are made concerning the role these surface charging mechanisms may play in the adhesional behavior of lunar materials.

Key Words: Adhesion, Ultrahigh Vacuum, Silicates, Moon, Dislocation, Space Charge, Impurity Distributions, Cleavage, Polarization.

# Production of Surface Electrostatic Charging on Dielectrics Cleaved in Vacuum: Theoretical

J. J. Grossman*

## Introduction

Ryan and Baker (this conference) [1] have observed the formation of considerable surface charging for silicates cleaved at $10^{-10}$ torr. This charging is stable, apparently non-uniform on a macroscopic scale, persists to $10^{-4}$ torr and contributes significantly to the adhesion. Additional observations have been that the resultant force field is of such a nature that it can rotate the samples into alignment, and that while on some occasions the samples are attracted to any metal in the vicinity, on other occasions there is no attraction.

The long range force which attracts and aligns cleaved samples is assumed to be electrostatic since no other known forces which could act are attractive at 1-2 mm separations.

Attraction of some samples to the grounded metal chisels indicates that either the net charge on each half of the cleaved silicate is not zero, or the separation between positive and negative regions is large enough to induce a dipolar image charge in the metal to which it then is attracted.

Some samples which exhibited long range attractive forces when brought into contact also exhibited rotational and translational reorientation back to their pre-cleavage alignment. This suggests that the charging on mating samples consists of dipolar or multipolar distributions which are complimentary to one another on the mating cleavage faces.

The hypothesis explored in this paper is that the cleavage plane intersects a polarization field $\vec{P}$ in these insulating silicate crystals which has non-zero components perpendicular to the cleavage plane $\vec{P} \cdot \vec{n} = 0$ where $\vec{n}$ is the unit normal vector to the cleavage plane. This peper considers, qualitatively, mechanisms which could be responsible for this charging; in particular, the monopolar and dipolar structure of individual dislocations and dislocation arrays associated with stress fields and with charge mosaics produced by non-uniform impurity distributions.

In the following sections the monopolar and dipolar structure of edge dislocations is illustrated using the fcc alkali halide lattice as an example. The theory of Eshelby et al [2] of a cylindrical space charge cloud surrounding an edge dislocation is extended to include a dipole structure because lattice symmetry is lower in the vicinity of the dislocation. Then, internal polarization fields produced by organized motion of dislocations in stress fields is discussed. Cleavage through the field leaves a net surface or volume charge if the relaxation time is sufficiently long. Next the origin of internal polarization fields due to non-uniform impurity distributions is related to the position of the Fermi level in the forbidden energy-band-gap. Then, the proposed, theoretical models are discussed in relation to the experimentally observed charging effects. Finally, some brief comments are given on the role these various processes may play at the lunar surface.

## Surface and Edge Dislocation Charge Distributions

### Space Charge Distribution at a Crystal Surface

Lehovec [3] treated non-uniform charge distributions in ionic crystals based on model suggested by Frenkel [4]. He considered the space-charge layer

produced at the surface of a crystal due to Frenkel and Schottky defects. The theory is summarized here because it is fundamental to what follows.

If the number of lattice defects in a crystal is sufficiently small, the Gibbs potential of the $i^{\underline{th}}$ component $G_i$ is, to a good approximation, a logarithic function of the concentrations $N_i$.

$$(\delta G_i / \delta N_i) = E_i + kT \ln (N_i / Z_i) \tag{1}$$

where k is the Boltzman constant, T is the absolute temperature, $E_i$ is the heat of reaction, and $Z_i$ is the number of possible positions of particles of type i. When a defect is transported from the surface at the reference potential V = 0 to some point x in the crystal where the electrostatic potential is V(x) due to the space charge near the surface, the heat of reaction will be

$$E_i = u_i + q_i V(x) \tag{2}$$

Let $N_+$ and $N_-$ be the bulk concentrations of interstitial cations and anions and $V_+$ and $V_-$ be the concentration of cation and anion vacancies.

Then

$$N_+ = 2Z \exp[(-u_1 - eV)/kT] \tag{3}$$

$$N_- = 2Z \exp[(-u_2 + eV)/kT] \tag{4}$$

$$V_+ = Z \exp[(-u_3 - eV)/kT] \tag{5}$$

$$V_- = Z \exp[(-u_4 + eV)/kT] \tag{6}$$

(The Convention used is that interstitial ions are transported from the surface to the interior whereas for vacancies, a lattice ion is transported from the bulk to the surface). The space charge density is

$$\rho = e[N_+ - N_- + V_+ + V_-] \tag{7}$$

which is just compensated by the complementary surface charge. The magnitude of the space charge density close to the surface is

$$\rho \ll ze \tag{8}$$

when $U_1 \ldots U_4 \gg kT = 25$ mV at 25°C. The crucial points, when starting with a perfect lattice, are

(a) If the energy of formation of interstitial cations is less than interstitial anions, more interstitial cations will form and migrate into the interior than interstitial anions.

(b) If the energy to transport positive lattice ions from the bulk to the surface is less than the transport of negative lattice ions, then the greater number of $V_+$ lattice vacancies will be created than $V_-$ vacancies.

(c) The migration of interstitials (process "a" above) would leave the surfaces negatively charged while the migration of lattice ions to the surface (process "b" above) would leave the surface positively charged. The net charge is a combination of these two processes.

(d) The presence of impurities modifies the equilibrium concentrations of vacancies and interstitials [5].

An exact solution for the potential function was found for surface charging by Frenkel [3] and Lehovec [2] and it is given in appendix A. The important result is that for the NaCl ionic lattice the bulk potential is

$$V_\infty(NaCl) = -0.28\ eV \tag{9}$$

which corresponds to an excess of $Na^+$ ions on the surface of the crystal and a negative space charge cloud in the surface region corresponding to $Na^+$ ion vacancies. The penetration of the space charge layer is found to be

$$\lambda(cm) = 1.1 \times 10^{-10} \sqrt{T}\ \exp(5400/T) \tag{10}$$

and the surface charge density

$$Q = (\epsilon\epsilon_0 kT/\lambda)\sqrt{8}\ \sinh(eV_\infty/2kT) \tag{11}$$

At $T = 600^\circ K$, $Q = 1.6 \times 10^{11}$ charges/$cm^2$. At room temperature the space charge region is .15 cm deep which is comparable to the distances over which the long range forces are observed to act.

Monopole Structure of Edge Dislocations

Eshelby et al [2] analyzed Pratt's [6] suggestion that dislocations, excluding perfect screw dislocations, in ionic crystals should be charged by having an excess of jogs of one sign surrounded by a sheath of vacancies of predominantly the opposite sign. In essence, the edge dislocation may be considered a one dimensional surface which emits vacancies into the bulk of the crystal. This establishes an electric field which is similar to the surface space charge layer treated by Lehovec. The analogy is even more apparent by considering the transition sequence from an isolated edge dislocation to a planer array (which is a low angle grain boundary), to a large angle grain boundary, and finally separation into independent crystal surfaces.

The electrical structure of the dislocation is therefore a monopole line charge ( $\sigma$ charges/cm) surrounded by a compensating vacancy atmosphere. The mathematical problem based on Poisson's equation is similar to Lehovec's crystal surface equation 3 (appendix A) namely

$$\nabla^2 p = 2\lambda^2 \sinh p \tag{12}$$

with the new boundary conditions required for a line charge. Eshelby et al give the solution for small values of $p = e\,(V - V_\infty)/kT$ in terms of the modified Bessel Function

$$p = (2\sigma/\epsilon) K_0(\kappa r) \tag{13}$$

where $\kappa^2 = \frac{8\pi e^2}{\epsilon kT}\,(N_+ + V_-)$ is connected to Lehovec's parameter $\lambda$ by $\kappa\lambda = \sqrt{2}$ . Recently Koehler, Langreth and Von Turkovich (1962) [7] have given a more detailed analysis.

Physical Structure of f.c.c. Edge Dislocations

Certain geometrical properties of edge dislocations should be discussed before the electrical theory can be extended. More explicitly, the [001] edge dislocation in a fcc lattice of the NaCl is chosen as an example, Figure 1. It is formed by removing a semi-infinite pair of adjacent $(1\bar{1}0)$ planes beginning at the slip plane. In the (001) plane shown a $[1\bar{1}0]$ line of $Na^+$ ions (small circles) and an adjacent line of $Cl^-$ ions (large circles) are removed. In the next lower or upper (001) plane the $Na^+$ and $Cl^-$ ions interchange positions. This alternation of ions continues in succeeding planes. Therefore, to the order of approximation considered here, the perfect edge dislocation is electrically neutral, though as discussed later a dipolar charge is actually present also.

Motion of a [001] dislocation is shown schematically in Figure 2. The dislocation core is comprised of three $Na^+$ ions and three $Cl^-$ ions distributed in the form of a distorted hexagon on four (110) planes, two above and two below the slip plane. Under stress, one $Na^+$ - $Cl^-$ ion pair on adjacent planes above and below the slip plane, interchange positions moving a distance $a\sqrt{2}/4$ through the stressed intermediate configuration shown in Figure 2b.

When a dislocation emits a vacancy, an ion (a $Na^+$ ion in the case shown in Figures 3) moves into the center of the dislocation core just below the slip plane. The vacancy which diffuses away from the dislocation forms part of the compensating space charge atmosphere which surrounds the ion in the center of the dislocation. The new configuration which places a charge on the dislocation line is identical with that in Figure 2b except that the slip plane is $1/4\,[1\bar{1}0]$ lower (Figure 3). In the static case, then, the charge center may be considered to be $180^\circ$ out of phase. Alternatively, when the dislocation moves along a given (110) slip plane, the charge center associated with the dislocation moves along a slip line parallel to the (110) slip plane but displaced $1/4\,[1\bar{1}0]$ below this plane. If the sequence of configurations for the dislocation is represented as a, b, a' then the corresponding sequence for the charge center is b,a,b'.

Calculations of the lattice distortion surrounding dislocations in ionic fcc crystals have been carried out by Huntington et al (1955), [8] and Bassani and Thomson (1956) [9]. In both investigations, association energies are calculated for impurities and vacancies interacting with edge and screw dislocations. Although Bassani and Thomson use a potential function which recognizes differing ionic radii for the positive and negative ions, Table 1,

TABLE 1A

Effective Ionic Radii of Alkali Halide Ions in Angstrom Units

| | | | |
|---|---|---|---|
| $Li^+$ | .60 to (.78) | $F^-$ | 1.36 |
| $Na^+$ | .95 | $Cl^-$ | 1.81 |
| $K^+$ | 1.33 | $Br^-$ | 1.95 |
| $Rb^+$ | 1.48 | $I^-$ | 2.16 |
| $Cs^+$ | 1.69 | | |

TABLE 1B

Ratio of Cation to Anion Radii

| | $F^-$ | $Cl^-$ | $Br^-$ | $I^-$ |
|---|---|---|---|---|
| $Li^+$ | .45 | .33 | .31 | .28 |
| $Na^+$ | .70 | .52 | .49 | .44 |
| $K^+$ | .98 | .73 | .68 | .61 |
| $Rb^+$ | 1.04 | .82 | .76 | .69 |
| $Cs^+$ | 1.24 | .94 | .87 | .78 |

they computed positions only for ions in the configuration shown in Figure 1. If we can assume that larger diameter ions are forced from regions of high stress to regions of low stress while the reverse is true for smaller diameter ions, then ions on adjacent (001) planes will be displaced as shown schematically in Figure 4. The net effect is that line dipoles are produced at each of the six positions surrounding the dislocation core[1]. These dipoles can be significant because each atomic plane contributes three dipoles as compared with one monopole charge per hundred atoms along the dislocation line.

The solution for the space charge field produced by the dipole structure due to the dislocation is more difficult than the monopole solution (for reasons similar to those given by Eshelby). A particular solution for the potential given in a form that the monopole and dipole cases can be compared is

$$V = V_M + V_D = \frac{2\sigma}{\epsilon}\left[K_o(\kappa r) + \kappa a \cdot \frac{\alpha_D}{\alpha_M} K_1(\kappa r)\cos\phi\right] \qquad (14)$$

where a is the lattice spacing, $\alpha_D/\alpha_M$ is the ratio of the number of dipoles to monopoles per unit length of dislocation, $K_o(x)$ and $K_1(x)$ are the modified Bessel function of orders zero and one respectively, and $\phi$ is the angle between the radius vector $\vec{r}$ and the dipole moment vector $\vec{m}$. A detailed analysis of these factors is beyond the scope of the present paper except to note that $\kappa a$ is of the order of $10^{-2}$ to $10^{-5}$ whereas $\alpha_D/\alpha_m$ can vary from $10^2$ to $10^5$. We conclude that the dipole field, in certain circumstances, can make a significant contribution to the space charge distribution.

Another feature of the dislocation which was mentioned previously is that it lacks a center of symmetry. Therefore in a stress field it will exhibit a

piezoelectric effect, and the dipole moment may be considered the net piezoelectric polarization induced by the internal stress field. External pressure should modify this dipole moment so that any distortion of a crystal should be accompanied by a corresponding change in the polarization field.

## Polarization Fields in Homogeneous Solids

Plastic deformation, dislocation climb and polygonization, which produce slip bands and other non-uniform density arrays, are well known [10, 11, 12]. These ordered and disordered textures are time dependent on parameters such as the stress field, temperature, deformation rate and the slip bands of the specified material. Dislocation pileup, multiplication, interaction, etc., are processes which are assumed to be an integral part of any given sample's history, especially with natural minerals.

In the following discussion, the final dislocation distributions and orientations will be assumed without attempting a detailed analysis of the steps which could produce them. Instead, the focus will be on the electronic charge distribution associated with dislocation arrays and the types of long range electrostatic fields which can be produced by cleavage near or through the array.

## Dislocations in Thermal Equilibrium

The trivial case, cleavage of a perfect, non-piezoelectric crystal, is one which cannot produce strong surface charging. During formation of the surface space-charge layer by vacancy migration, the net external field is always zero. However, a repulsive dipole field is produced at the edges of the crystal which would tend to prevent the crystal halves from returning to their original positions, Figure 5.

Monopole arrays can produce surface charging if the plane of the monopole distribution is not perpendicular to the cleavage plane. A dislocation array is represented schematically in Figure 4 by a plane intersecting the cleavage plane. It can be a grain boundary, low angle grain boundary or glide bands produced by cross-slip.

The net surface charge after cleavage is due to the uncompensated charges in the ion atmosphere at the intersection of the cleavage and dislocation planes. If $\theta$ is the angle between the planes and $\kappa^{-1}$ is the width of the ion atmosphere, Figure 6, then the width of the attractive space charge region w is

$$w = \kappa^{-1} \csc \theta \tag{15}$$

If the angle is $0^{\circ}$, the crystal containing the dislocation plane has a net charge with the same sign as the dislocations. The net charge (equal and opposite on the two faces) will be different from zero whenever the cleavage plane is closer to the dislocation plane than $1/\kappa$, the width of the ion atmosphere.

The single slip plane in Figure 6 produces a dipole surface layer. Figure 7 shows a pair of dipoles produced by cross slip. Figure 8 shows a complex multipole structure due to dislocation bands produced whenever the zone axes of intersecting slip bands also intersect the cleavage plane.

In each of the previous cases, it was implicitly assumed that the dislocations are randomly oriented, i.e., there are an equal number of positive and negative dislocations. Anisotropic stress fields and processes such as polygonization can produce an excess of dislocations with the same sign. Figure 9 shows schematically the polarization field produced by the dipole moments of ordered

dislocations of a doubly deformed, polygonized crystal. In this case the monopole charge plays no role whatsoever in surface charging.

Non-Equilibrium Effects

At sufficiently low temperature, the space charge surrounding the dislocation remains fixed in the crystal matrix as an external stress moves the dislocation from its original position [2,8]. The dislocation motion carries with it a charge which can be observed as a measurable current [13, 14, 15, 16, 17]. A dipolar charge distribution can be generated by motion of dislocation bundles which leaves behind the space charge cloud which initially surrounds them. Simultaneously new dislocations, generated by dislocation multiplication processes, emit immobile vacancies which add to the initial space charge density. Intersection of this polarization field by the cleavage plane produces a surface charge, Figure 10.

Inhomogeneously Doped Crystal Effects

Homogeneous crystals which have been considered in the previous sections include, implicitly, crystals with uniformly distributed impurities. The net charge on the edge dislocation depends on the dopant [18, 19]; for example, NaCl doped with $Ca^{++}$ produces a higher positive charge per unit length than undoped crystals, whereas $OH^{-}$ ions will charge the dislocation negatively [16].

The Fermi level or chemical potential in an annealed crystal is everywhere constant whereas the energy difference between the valence band edge and the Fermi level changes with composition, Figure 11. A well-known consequence is the built-in electric field in the transition zone between regions of varying impurity density [20, 21, 22]. The electric field compensates the diffusion

force due to the charge carrier concentration gradient. Therefore, a cleavage plane through an inhomogeneous crystal region must intersect a polarization field as long as the concentration gradient does not lie in the cleavage plane. The cleaved sections may or may not have a net electrical charge which depends on the complexity of the impurity distribution.

## Discussion

The pertinent experimental evidence which forms a framework for understanding the long range electrostatic forces in vacuum cleaved silicates can be divided as follows:

a. Direct Measurement of Surface Charge - Deryagin and Metsik [23]

b. Adhesion of Mica - Bryant [24]

c. Minimum Yield Stress - Eshelby et al [2]

d. Direct Measurement of Current Flow During Crystal Deformation

e. UHV Measurement of Long Range Attraction - Ryan and Baker [1]

f. Theory of Junctions in Semiconductors and Insulators

Deryagin and Metsik [23] found variations in the electrostatic charge on a mica surface during cleavage which they found was sensitive to water vapor. Bryant's calculations [24] agreed with the observed increase in mica adhesion from 260 ergs/cm$^2$ in air to 2000 ergs/cm$^2$ in vacuum if he assumed that the increase was due to the electrical work done in separating a mosaic of electrical charge on the cleavage surfaces. In air the high polarizability of water was assumed to disrupt an undefined process which induced organized transfer of cations to one of the two surfaces newly formed by the mica cleavage. Since the energy of cohesion can be decreased by a factor of ten by the cleavage environment, the origin of the polarization field which organizes cation transfer into large area mosaics is a significant problem.

Non-uniform impurity distributions in mica are known. Figure 12 shows shallow etch pits due to impurities, edge dislocations in relatively low density, and hillocks due to etching inhibition by impurities. The charging effects in mica are most easily explained, therefore, by variations in the impurity distributions in the crystals. In contrast to mica, the dislocation density in network silicates used in Ryan's work, is very high, Figure 13. In this case charge effects associated with dislocations are important.

Eshelby derived the charged dislocation theory to show that the yield strength of ionic crystals varied as a function of the work required to move a dislocation out of its compensating charged vacancy cloud. This could be controlled by doping the crystal and/or varying the temperature. Isoelectric points were found as minima in the yield-stress which corresponded to neutral dislocations.

A number of direct measurements of the currents associated with moving dislocations were inspired by Eshelby's theory [References 15-18]. Most convincing is probably the work of Froelich [16]. In this investigation, the dislocation is made to carry an unambiguous charge which is either positive (pure or $Ca^{++}$ doped NaCl) or negative ($OH^{-}$ doped NaCl). The central region from which the dislocations migrate takes on a charge opposite to that carried by the moving dislocations.

The attractive and repulsive forces to be expected from dislocations and non-uniform impurity distributions is summarized in Table 2. Ordered and disordered arrays are important for neutral dislocations since the dipole moments of equal numbers of positive and negative dislocations just cancel each other. In this case only a repulsive force can be observed due to the dipole structure

TABLE 2

Theoretical Surface Charge Distributions Associated

With Edge Dislocations and Impurity Distributions

| | Angle Between Cleavage Plane and Disloc. Array | ATTRACTIVE FORCE | | | | REPULSIVE FORCE | | | |
|---|---|---|---|---|---|---|---|---|---|
| | | Monopole | | Multipole | | Monopole | | Multipole | |
| | | Annealed | Stressed | Annealed | Stressed | Annealed | Stressed | Annealed | Stresse |
| 1. Neutral Dislocations | | | | | | | | | |
| A. Disordered Arrays | | No | No | No | No | No | No | Yes | Yes |
| B. Ordered Arrays | ∥ | Yes | Yes | Yes | Yes | No | No | No | No |
| | ∢ | P* | P | P | P | No | No | P | P |
| | ⊥ | No | No | No | No | No | No | Yes | Yes |
| 2. Charged Dislocations | | | | | | | | | |
| | ∥ | P | Yes | P | Yes | No | No | No | No |
| | ∢ | P | P | P | P | No | No | P | P |
| | ⊥ | | No | No | No | No | No | Yes | Yes |
| 3. Non-Uniform Impurity Distribution | | Yes | - | Yes | - | No | - | No | - |

P = Possible

at the cleavage perimeter which will prevent realignment of the perimeter. An induced dipole attraction of the perimeter dipole on the face would be attractive. However, it is doubtful that this could be observed experimentally.

The line dipole structure of neutral dislocations generates a polarization field when grouped into ordered arrays. When the dislocations are perpendicular to the cleavage plane a repulsive force is produced. Attractive forces depend on the angle between the array polarization field and the cleavage plane. The attractive force is zero (repulsive force maximum) if the dipole moment is perpendicular to the cleavage-plane normal, and the maximum when parallel. In between, the net force can be repulsive or attractive. Multipole distributions are possible due to non-uniform strains which order the dipoles differently in adjacent regions of the crystal.

Charged dislocations in stressed crystals produce a similar behavior. The force between cleavage faces is repulsive when the cleavage planes and dislocation array planes are perpendicular and the force is attractive when the planes are parallel.

Charged dislocations act differently when annealed. In this case, the repulsion is weaker and the attractive force covers a mosaic area which extends only $1/\kappa$ from the dislocation array plane. If the cleavage is to dislocation array plane is larger than $1/\kappa$ no attraction will be observed. Therefore, the monopole attractive force, when it exists in annealed specimens, will always be weaker than in stressed crystals.

Non-uniform impurity distributions produce only attractive forces independently of stress. Ryan and Baker have observed UHV silicate cleavages with no long

range forces, monopole attraction to metal objects in the vicinity and multipole orientation of mating, cleaved surfaces. It is not possible to say whether lack of observation of long range forces in some cases is due to the absence of charge mosaics or whether it is the null resultant of compensating repulsive and attractive fields.

In cases where the high, initial attractive force decreases within minutes after cleavage to a stable intermediate value, two effects are important. First, there is adsorption of background gas (gas bursts have been noted often which come primarily if not entirely from the chamber walls) which neutralizes the field external to the crystal by polarization, or by surface ionization, ion migration and charge compensation. Second, charge separations produced by stress during the cleavage process will relax, depending on bulk crystal, dislocation, surface and grain boundary conductivities, in times which should be in the range 1 sec to a few hours [18, 19]. Here again, insufficient data is available at present to decide unambiguously if one or both mechanisms are operative. Although the long range, UHV attractive force persists for weeks, it becomes immeasurably small as the pressure is raised above $10^{-4}$ torr.

## Implications of Electrostatic Surface Charging to the Moon

Natural or future man-induced disruption of material on the moon will produce surface electrostatic charging in the existing ultrahigh vacuum. Factors which relate to the magnitude of this effect with lunar material are the relative density of dislocations and impurity density gradients when compared with minerals found on earth, and the environmental conditions which contribute to discharging the electrostatic fields.

Impurity density gradients in lunar insulators should be essentially the same

as those found in earth minerals even though there is probably some difference in average composition. Differences may be expected, however, from the higher point and cluster defect densities produced by cosmic rays and the solar winds which penetrate the surface layer to varying depths. The flux of meteorites and micrometeorites should induce a higher dislocation density in lunar surface minerals due to shock metamorphism.

Cosmic rays, the solar wind, and solar photons (UV, X-rays and $\gamma$-rays) each contribute to the electrostatic discharge process. The sputtering component of the particle flux enhances surface diffusion whereas the radiation damage component increases bulk conductivity. Solar radiation decreases the electrostatic charging lifetime by photoconductivity, photoelectric emission and secondary electron emission. These latter discharging processes would decrease the charge lifetime regardless of the origin of the material, whereas the former, radiation damage and micrometeorite effects, will depend on the exposure time to the surface environment prior to cleavage.

## Conclusions

Long range electrostatic charging on cleaved surfaces of insulating crystals is found to be related to inhomogeneous impurity distributions and the monopolar and dipolar structure of edge dislocations. Stress dependent dislocation motion, crystal growth environment, and thermal history can produce attractive forces, repulsive forces, or a null force due to a compensating combination of both.

## Acknowledgement

I would like to acknowledge the valuable discussions with Dr. J. A. Ryan on silicate adhesion phenomena; with Dr. R. W. Willet on the dipolar structure

of the ion atmosphere surrounding edge dislocations, and Dr. D. H. Killpatrick, Dr. S. W. Benson and Mr. G. S. Berend on various aspects of the problem. I also would like to thank Mr. A. Phillips, Mr. V. Kerlins and Miss N. Tubbs for the electron micrographs of etched silicate replicas.

This research is supported in part by the Douglas Missile and Space Systems Division Internal Research and Development Program and in part by the National Aeronautics and Space Administration under Contract NAS7-307.

## Appendix A

The solution for the potential function starts with Poisson's equation

$$\nabla^2 V = -\rho/\epsilon\epsilon_o \qquad (A)1$$

($\epsilon$ is the dielectric constant, $\epsilon_o = 8.84 \times 10^{-14}$ amp sec/volt cm,) is in amp sec/cm$^3$, $\underline{x}$ in cm, and V in volts) using the boundary conditions that the potential V = 0 at the surface X = 0 and the potential gradient is zero in the bulk of the crystal. Then

$$-\rho(V) = 2e\left(N_+^{\infty} + V_-^{\infty}\right) \sinh p \qquad (A)2$$

where

$$p = e\left[V - V(\infty)\right]/kT \qquad (A)3$$

The exact solution of equations A1, A2 and A3 is

$$\ln\left[\frac{\exp(-p/2) + 1}{\exp(-p/2) - 1}\right] = \sqrt{2}\left(\frac{x}{\lambda}\right) + \ln\left[\frac{\exp(-p_o/2) + 1}{\exp(-p_o/2) - 1}\right] \qquad (A)4$$

where the length $\lambda$ is

$$\lambda^2 = \epsilon\epsilon_o kT/2e^2\left[N_1^{\infty} + N_4^{\infty}\right] \qquad (A)5$$

## References


1. J. A. Ryan and M. B. Baker, "Adhesional Behavior of Air and Ultrahigh Vacuum Formed Silicate Surfaces," This Conference, 1967.

   J. A. Ryan, "Adhesion of Silicates in Ultrahigh Vacuum," J. Geophys. Res., Vol. 71, No. 18, September, 1966, pp. 4413-4425.

2. J. D. Eshelby, C. W. A. Newey, P. B. Pratt and A. B. Lidiard, "Charged Dislocations and the Strength of Ionic Crystals," Phil. Mag., Vol. 3, 1958, pp. 75-89.

3. K. Lehovec, "Space-Charge Layer and Distribution of Lattice Defects at the Surface of Ionic Crystals," J. Chem. Phys., Vol. 21, No. 7, July 1963, pp. 1123-1128.

4. J. Frenkel, "Kinetic Theory of Liquids," Oxford University Press, London, 1946.

5. F. A. Kroger, "The Chemistry of Imperfect Crystals," North-Holland Publishing Company, Amsterdam, 1964.

6. P. L. Pratt, Inst. Metals Monograph and Report Series, Vol. 23, 1957, p. 99.

7. J. S. Koehler, D. Langreth, and B. von Turkovich, "Charged Dislocations in Ionic Crystals," Phys. Rev., Vol. 128, 1962, pp. 573-580.

8. H. B. Huntington, J. E. Dickey, and R. Thomson, "Dislocation Energies in NaCl," Phys. Rev., Vol. 100, No. 4, 1955, pp. 1117-1128.

9. F. Bassani and R. Thomson, "Association Energy of Vacancies and Impurities with Edge Dislocations in NaCl," Phys. Rev., Vol. 102, No. 5, June 1956, pp. 1264-1275.

10. A. H. Cottrell, "Dislocations and Plastic Flow in Crystals," Oxford University Press, London, 1953.

11. H. G. Van Bueren, "Imperfections in Crystals," 2nd Ed., North-Holland Publishing Co., Amsterdam, 1961.

12. J. Friedel, "Dislocations," Pergamon Press Ltd., London, 1964.

13. D. B. Fischback and A. S. Nowick, "Creation of a Potential Difference Across NaCl Crystals by Deformation," Phys. Rev., Vol. 98, 1955, p. 1543, Abstract K-7.

14. R. W. Davidge, "The Sign of Charged Dislocations in NaCl," Phil. Mag., Vol. 8, 1963, p. 1369.

15. A. Hikata, C. Elbaum, B. Chick, and R. Truell, J. Appl. Phys., Vol. 34, No. 8, 1963, pp. 2154-2158.

16. F. Froelich and D. Suisky, "Electrical Effects Induced by Moving of Dislocations in NaCl and KCl Crystals," Phys. Stat. Solidi, Vol. 4, 1964, p. 151.

17. I. Kishsh, "Study of Electric Effects Arising in Local Deformations of NaCl Crystals," Sov. Phys. - Cryst., Vol. 10, No. 8, May 1966, pp. 740-743.

18. K. L. Kliewer and J. S. Koehler, "Space Charge in Ionic Crystals. I. General Approach with Applications to NaCl," Phys. Rev., Vol. 140, No. 4A, November 1965, pp. A1226-A1240.

19. K. L. Klieiver, "Space Charge in Ionic Crystals. II. The Electron Affinity and Impurity Accumulation," Phys. Rev., Vol. 140, No. 4A, November 1965, pp. A1241-A1246.

20. N. F. Mott, and R. W. Gurney, "Electronic Processes in Ionic Crystals," 2nd Ed., Oxford Univ. Press, London, 1948.

21. W. Shockley, "Electrons and Holes in Semiconductors," D. Van Nostrand Co., Inc., Princeton, 1950.

22. H. K. Henisch, "Rectifying Semi-conductor Contacts," Oxford University Press, London, 1957.

23. B. V. Deryagin and M. S. Metsik, "Role of Electrical Forces in the Process of Splitting Mica Along Cleavage Planes," Vol. 1, No. 10; 1960, pp. 1393-1399.

24. P. J. Bryant, L. H. Taylor and P. L. Gutshall, "Cleavage Studies of Lamellar Solids in Various Gas Environments," Transactions of the Tenth National Vacuum Symposium, MacMillan Co., New York, October 1963, pp. 21-26.

## Footnote Page

* Principal Scientist, Lunar and Planetary Sciences Branch, Space Sciences Department, Douglas Aircraft Company, Santa Monica, California.

1. Additional relaxation may be possible if the six atoms in the core take on a "Z" configuration similar to the (111) zincblende structure.

## Figures

1. Structure of edge dislocation in fcc rock salt crystal perpendicular to the (001). Small circles represent $Na^+$ ions and larger circles $Cl^-$ ions (not to scale).

2. Motion of [001] edge dislocation in fcc rock salt lattice.

3. Schematic of edge dislocation emitting a $Na^+$ ion vacancy in fcc crystal.

4. Net dipole moment of edge dislocation produced by stresses acting on ions with different radii; fcc rock salt structure.

5. Dipole fringe field at the perimeter of a cleaved, homogeneous, single crystal with no dislocations.

6. Line dipole charge on cleaved surface due to plane array of charged dislocations.

7. Parallel line-dipolar surface charging due to cross slip.

8. Complex multipolar surface charging due to plane arrays of charged edge dislocations.

9. Polarization field produced by dipole moment of oriented edge dislocations.

10. Surface and volume charge distributions produced by plastic deformation. Edge dislocations carry positive charge.

11. Charge distribution and electric field produced by two different impurity levels in adjacent regions of a crystal.

12. Etch figures on cleaved mica (001).

13. Etch figures on orthoclase (001).

M-37729

# EDGE DISLOCATION IN FCC CRYSTAL; (001) PLANE

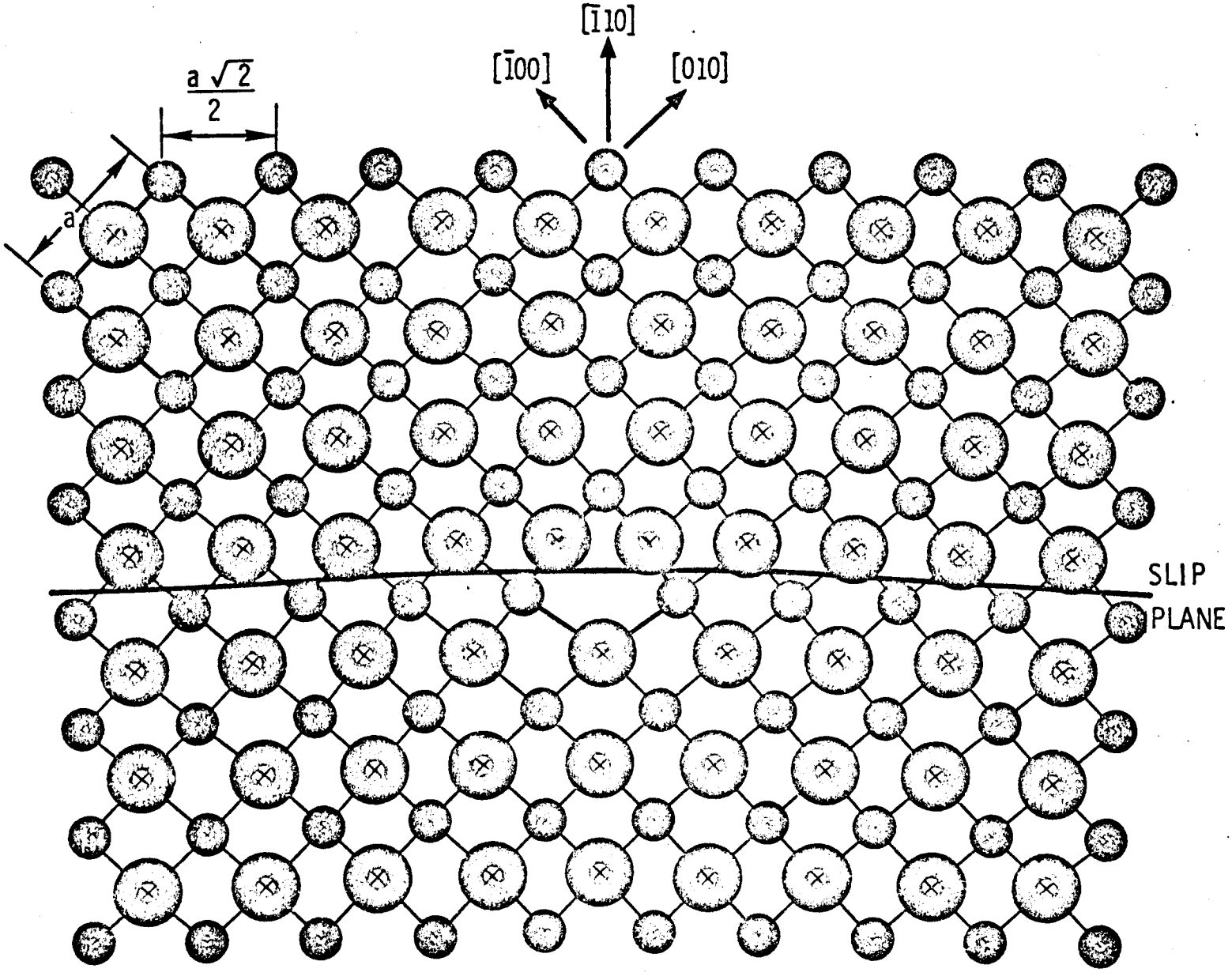


FIGURE 1

M-37728

# MOTION OF (001) EDGE DISLOCATION IN FCC LATTICE

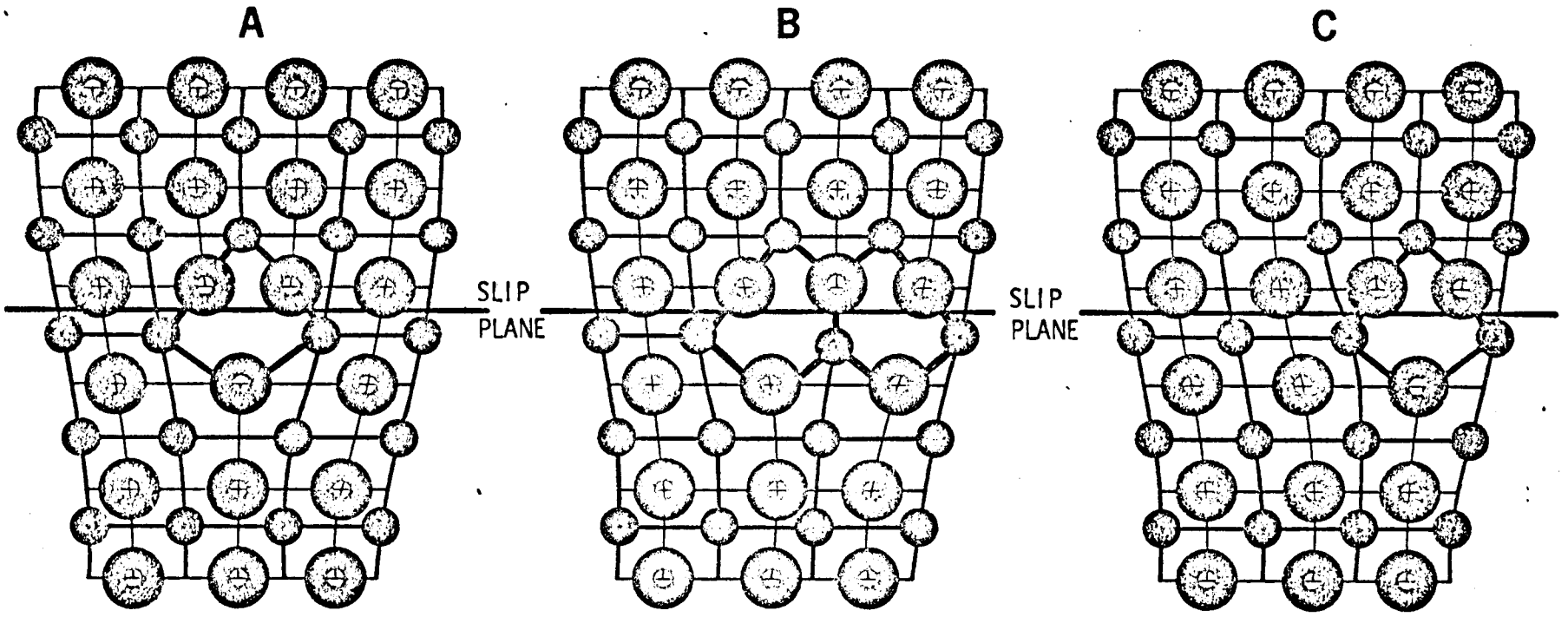


FIGURE 2

37717

M-37717

EDGE DISLOCATION EMITTING A $Na^+$ ION VACANCY IN FCC CRYSTAL

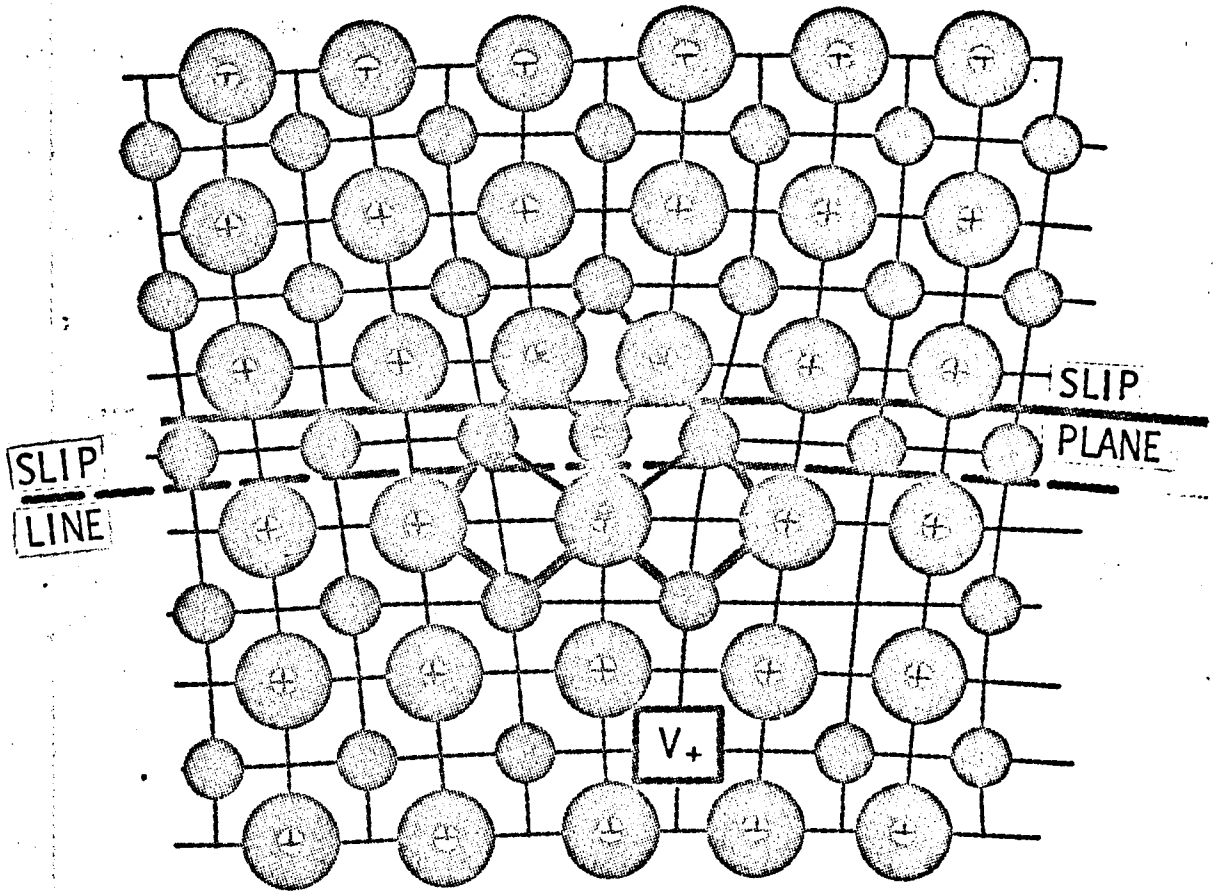


FIGURE 3

37722

M-37722

# NET DIPOLE MOMENT OF EDGE DISLOCATION; FCC ROCK SALT STRUCTURE

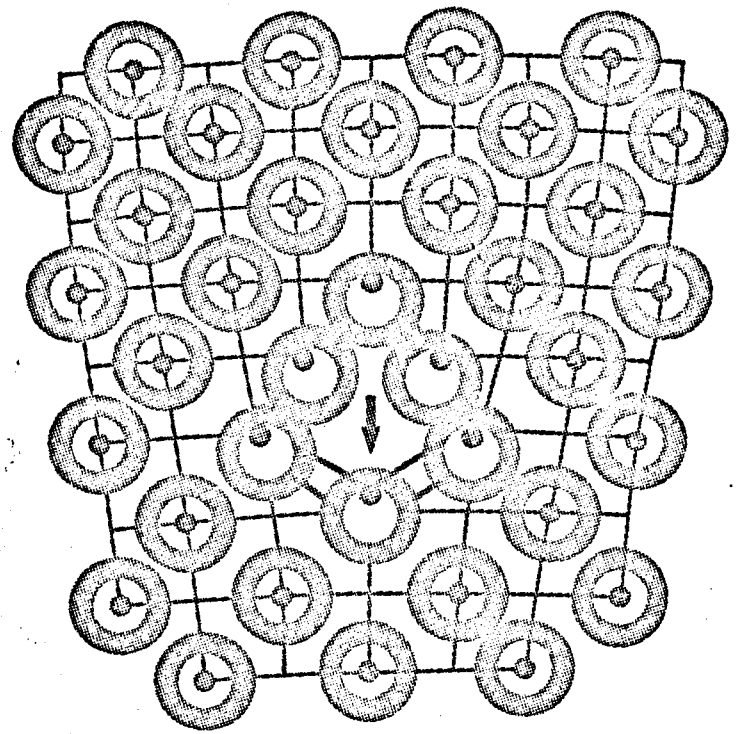

FIGURE 4

M-37718

# DIPOLE FRINGE FIELD IN CLEAVED, PERFECT CRYSTAL

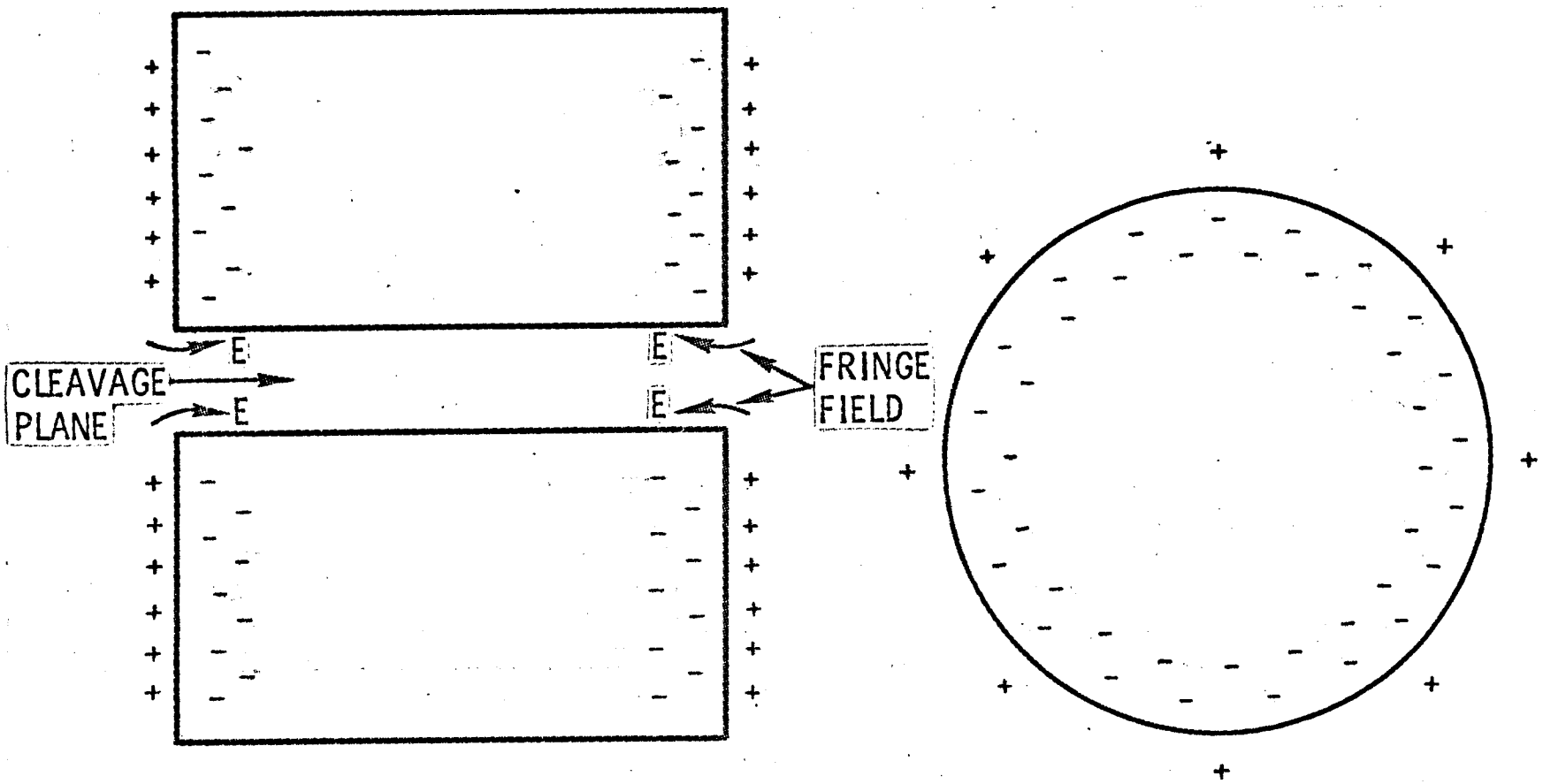


FIGURE 5

M-37727

# CHARGE DISTRIBUTION DUE TO PLANE ARRAY OF EDGE DISLOCATIONS

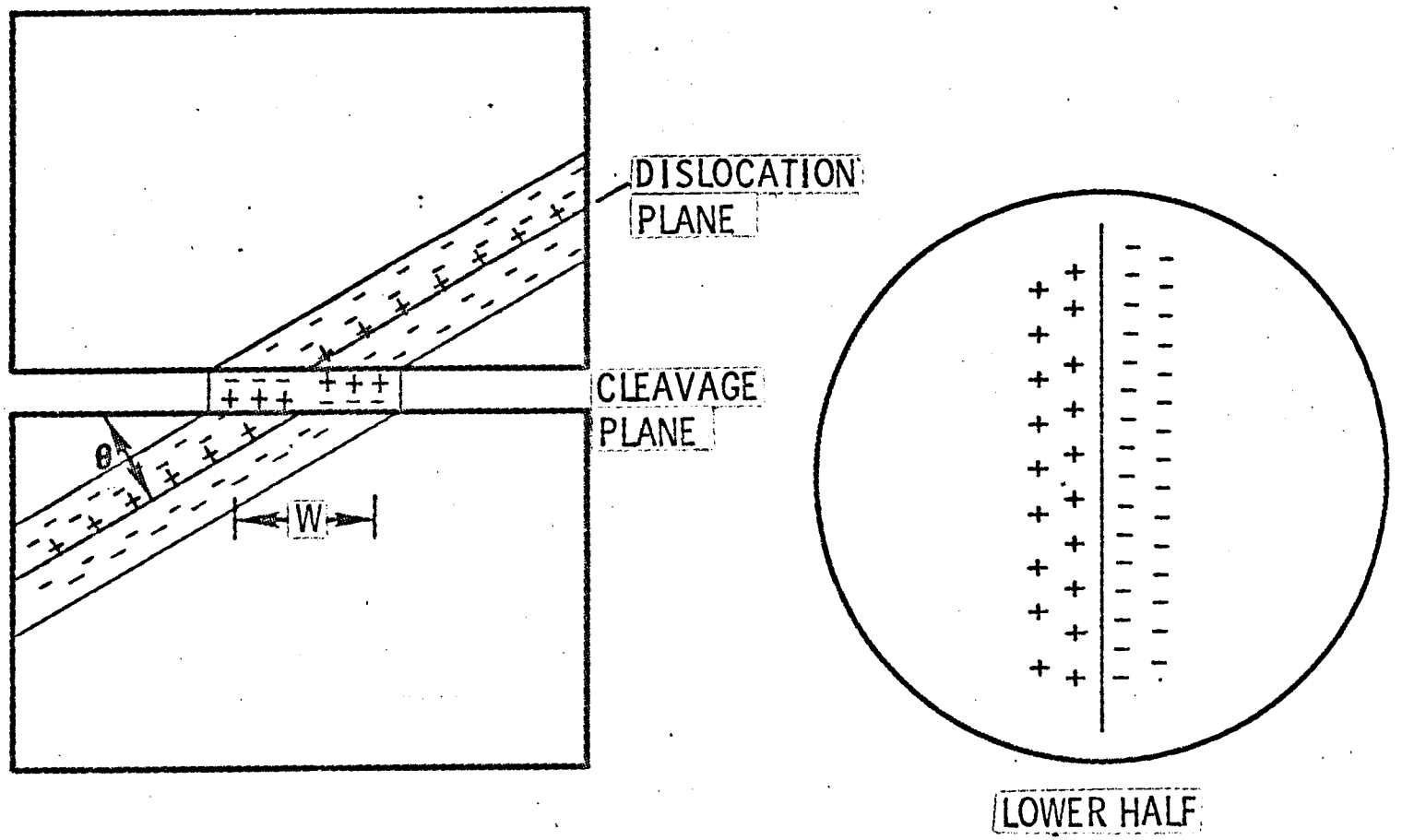


FIGURE 6

M-37719

# SURFACE CHARGING DUE TO CROSS SLIP

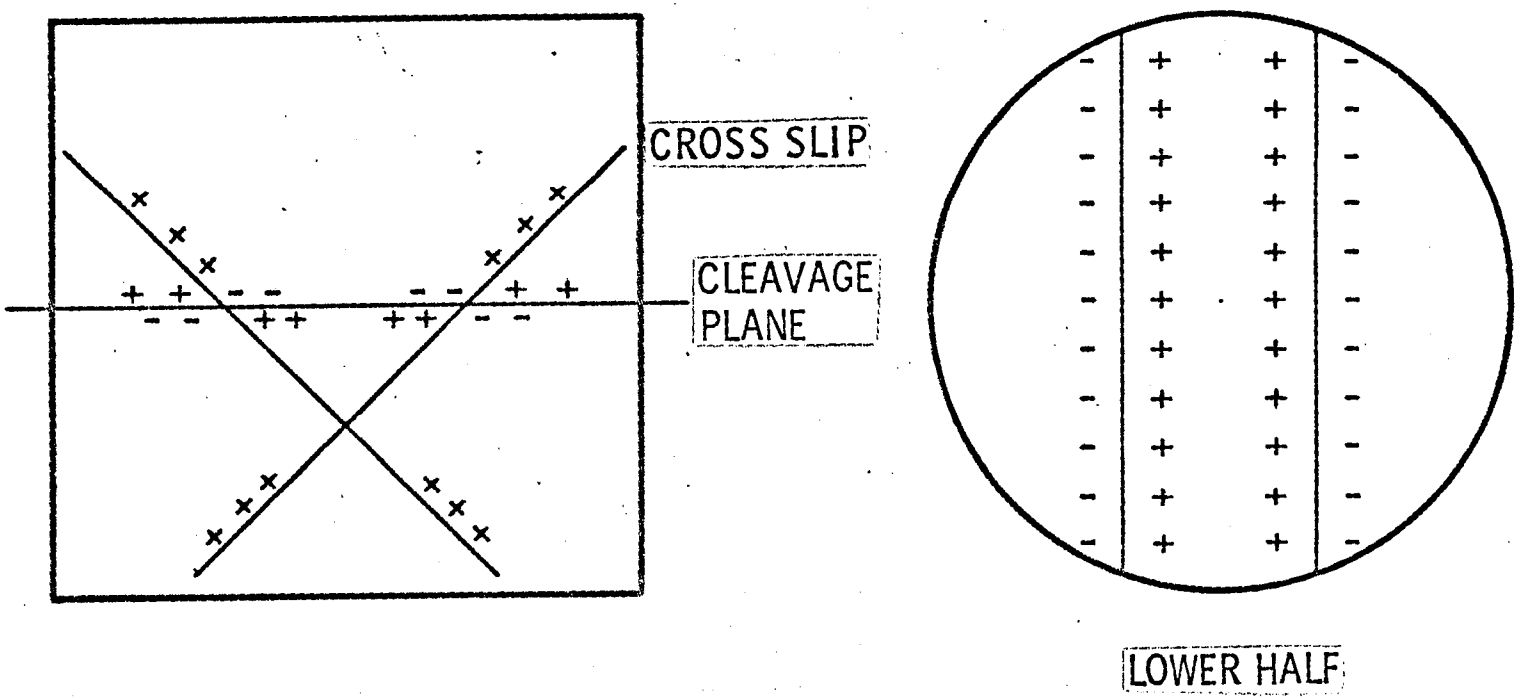


FIGURE 7

37723

M-37723

# COMPLEX MULTIPOLAR SURFACE CHARGING

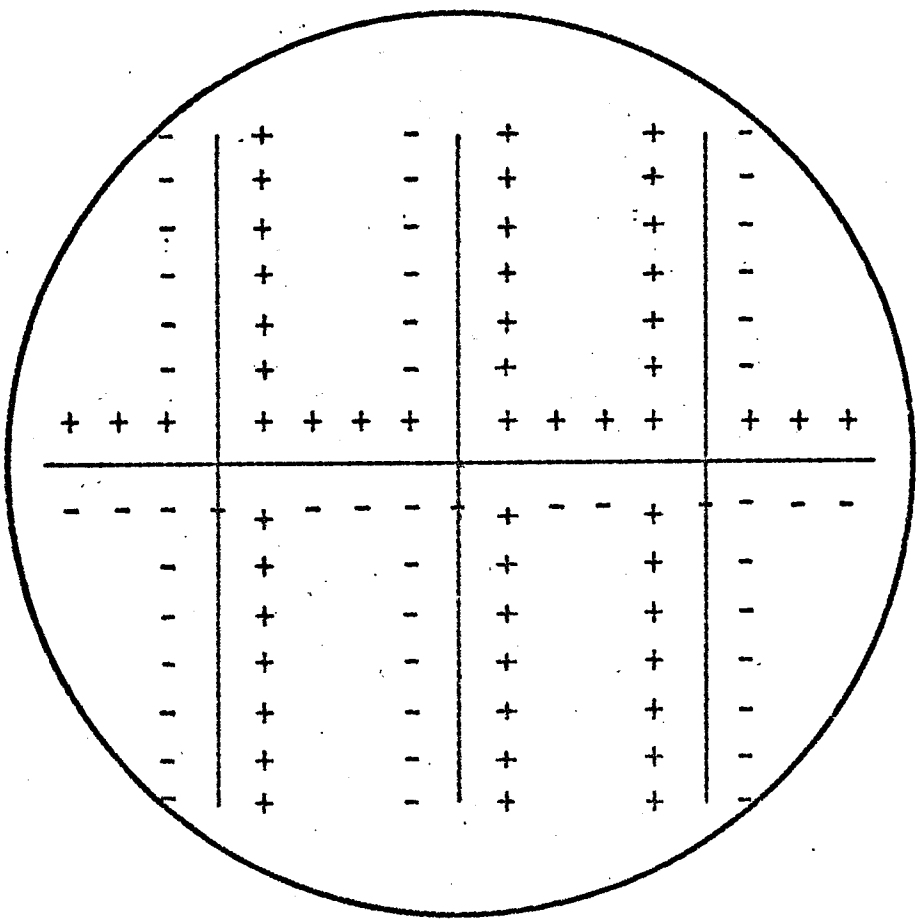

FIGURE 8

Appendix B



# Adhesional Behavior of Air and Ultrahigh Vacuum Formed Silicate Surfaces

By J. A. Ryan[1] and M. B. Baker[2]

To be presented at Adhesion of Materials in Aerospace Environments Symposium, May 1-2, 1967, Toronto, Canada

It is generally believed that the lunar surface consists primarily of silicates, and that these may exhibit significant adhesion under the ultrahigh vacuum conditions present. This paper presents results to date on a study of the possible adhesional behavior of lunar silicates. To place reasonable bounds on the range of lunar adhesional phenomena two types of silicate surface have been considered: the air-formed, or contaminated, surface and the vacuum-formed, or "clean", surface. It was found, for the air-formed surfaces, that the adhesion force was generally relatively low, in no case exceeding $5 \times 10^{2}$ dynes. Under low load the adhesion appeared to be due to the action of the dispersion forces, and was generally in the range $10^{-1}$ -1 dyne. At higher loads the adhesion force increased rapidly and appeared to be due to the action of the normal atomic bonding forces. It was found for the vacuum-formed surfaces that the adhesion force was much larger, and that a considerable amount of surface electrostatic charging was produced during surface formation. These results indicate that the range of lunar adhesional phenomena can be quite large.

Key words: Adhesion, Ultrahigh Vacuum, Silicates, Moon

# Adhesional Behavior of Air and Ultrahigh Vacuum Formed Silicate Surfaces

J. A. Ryan and M. B. Baker

## Introduction

The lunar surface is becoming an increasingly important part of the aerospace environment. Since the Moon lacks any appreciable atmosphere (the surface pressure is less than $10^{-10}$ torr) adhesion problems can be expected. These will in many ways be similar to those encountered in interplanetary space, but the Moon poses some very special problems of its own. In particular, we must not only be concerned with adhesion between mission components, but also with adhesion between these components and lunar material, and the adhesion of lunar material to itself (this latter determines how well the surface may support whatever structure we place upon it). This paper presents results of a study to determine what the adhesional behavior of lunar material may be.

It is generally believed that the lunar surface consists primarily of silicates. Silicates are an interesting group of materials for adhesion studies principally because they have properties which are significantly different from those of the materials studied most intensively in the past (the metals). Of note, their bonding is highly directional, they are dielectrics, and they exhibit a highly brittle behavior.

In order to determine the possible adhesional behavior of lunar silicates, we are faced with three fundamental questions: what is the nature of lunar silicates, what is the nature of lunar silicate surfaces, and what is the

rature of the surfaces of these terrestrial materials which we may take to the Moon? We do not presently know the types of silicates present on the Moon nor how the Moon's environment may affect their structures during formation. We can, however, minimize these uncertainties by chosing for study the most common of the terrestrial (and meteoritic) silicates and by utilizing only the most perfect specimens available (this reduces the effects of the Earth's environment subsequent to sample formation).

As for the nature of lunar silicate surfaces we can make a reasonable guess that they could range from ultraclean, where the charge and coordination demands are unsatisfied, to somewhat contaminated, where sufficient foreign material has been added (through adsorbtion and chemical reaction) to essentially satisfy the surface demands. Finally, the bulk of the materials we take to the Moon will arrive with a good part of their terrestrial surface contamination intact (i.e. oxide layers, hydrated layers). Subsequent exposure to the lunar environment, particularly to the solar wind, can cause a gradual surface cleaning and eventual complete removal of all terrestrial contamination. This contamination can also be removed by simple mechanical abrasion.

The general problem of lunar adhesion then becomes a case of measuring the adhesion between the materials involved utilizing the possible range of surface states. To date we have studied the adhesion of contaminated silicates contacting contaminated silicates and engineering materials, and clean silicates contacting clean silicates. The contaminated case was obtained by forming the contacting surfaces in air and subjecting them only to vacuum and heat. The "clean" case was obtained by forming the contacting surfaces at ultrahigh vacuum, by cleavage. The results for contaminated silicates contacting

M-37724

# DIPOLE POLARIZATION FIELD OF ORIENTED EDGE DISLOCATIONS

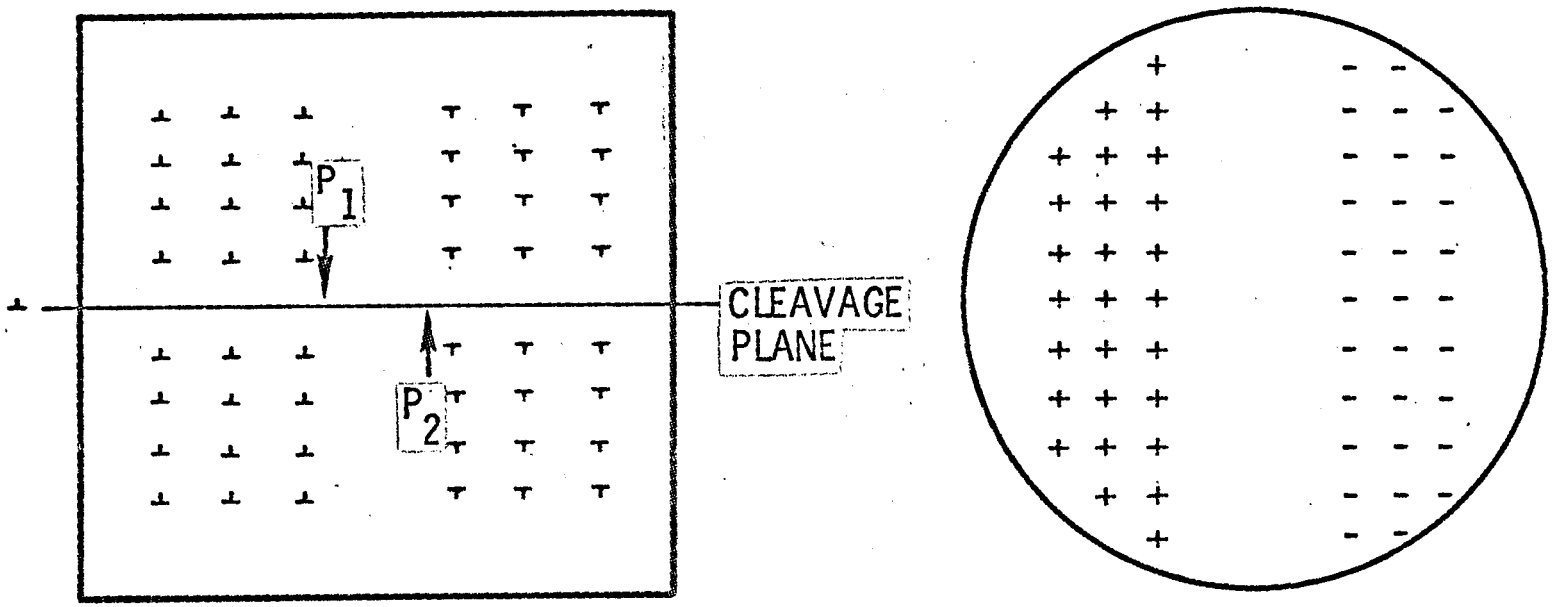


FIGURE 9

37720

M-37720

# SURFACE AND VOLUME CHARGE DISTRIBUTIONS PRODUCED BY PLASTIC DEFORMATION

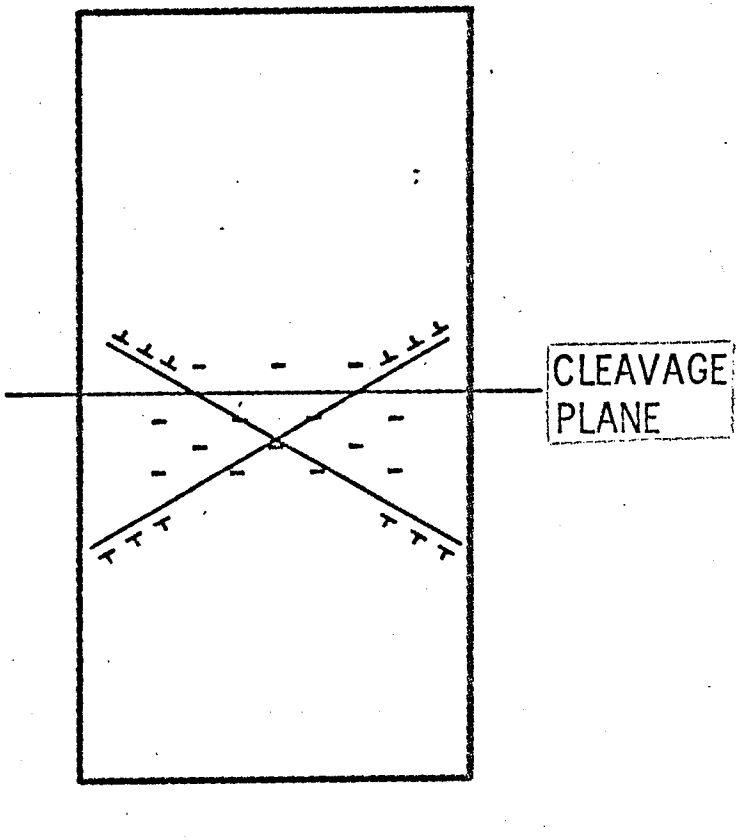


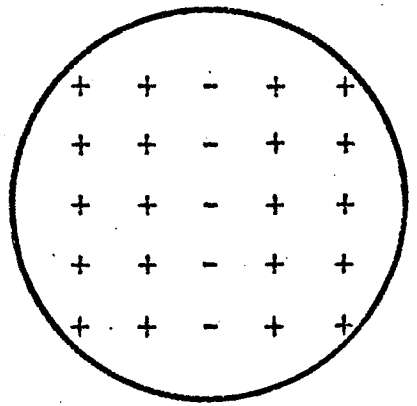

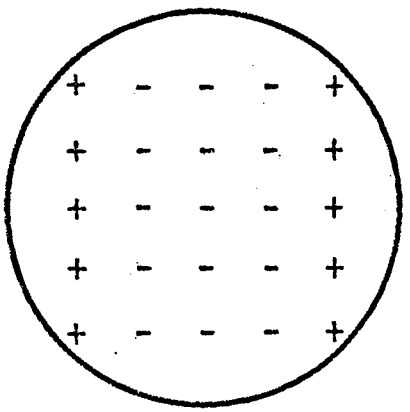

FIGURE 10

37721

M-37721

# ELECTRIC FIELD PRODUCED BY NON-UNIFORM IMPURITY DISTRIBUTION

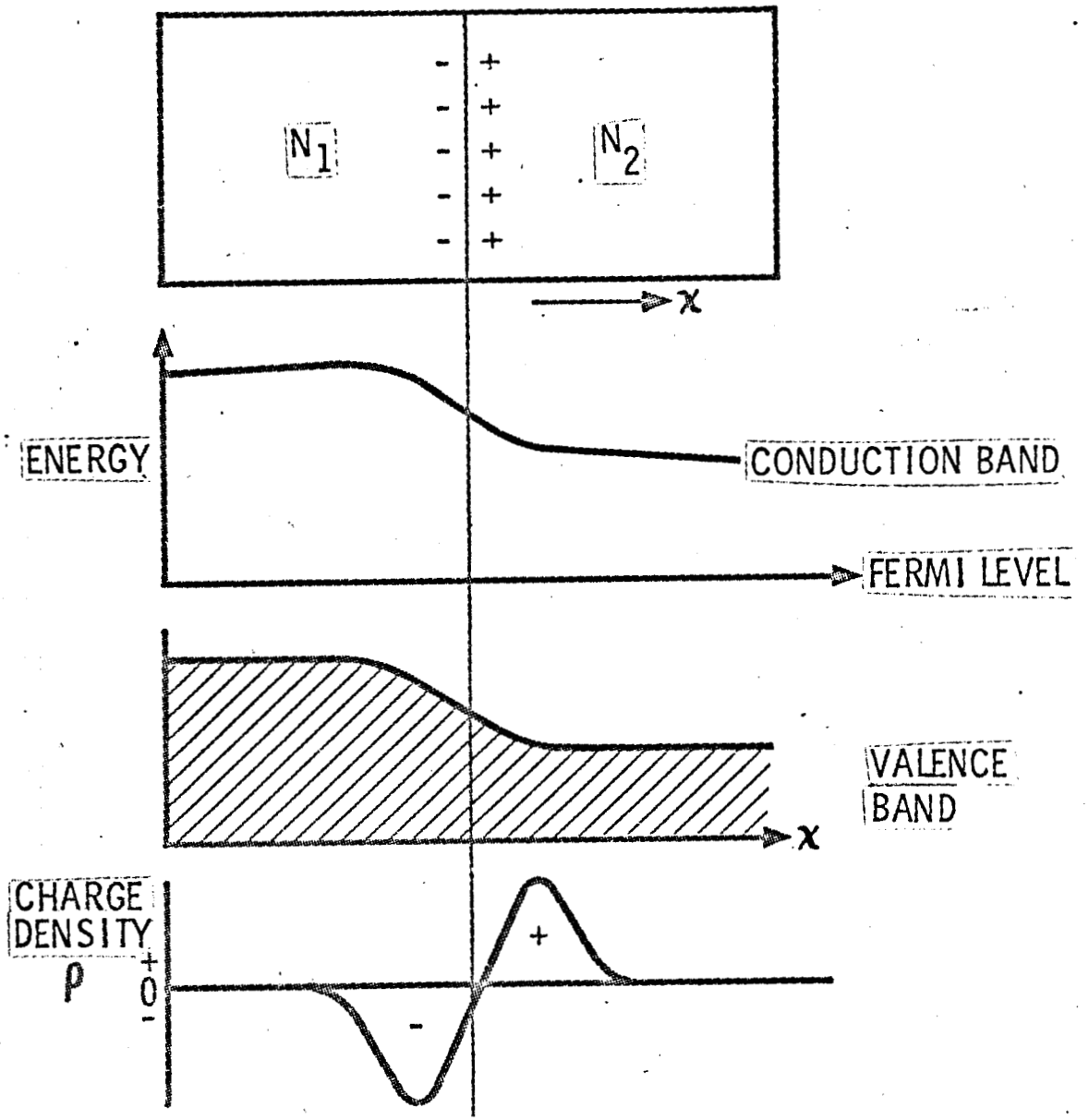


FIGURE 11

37725

M-37725

# ETCH FIGURES ON CLEAVED MICA (001)

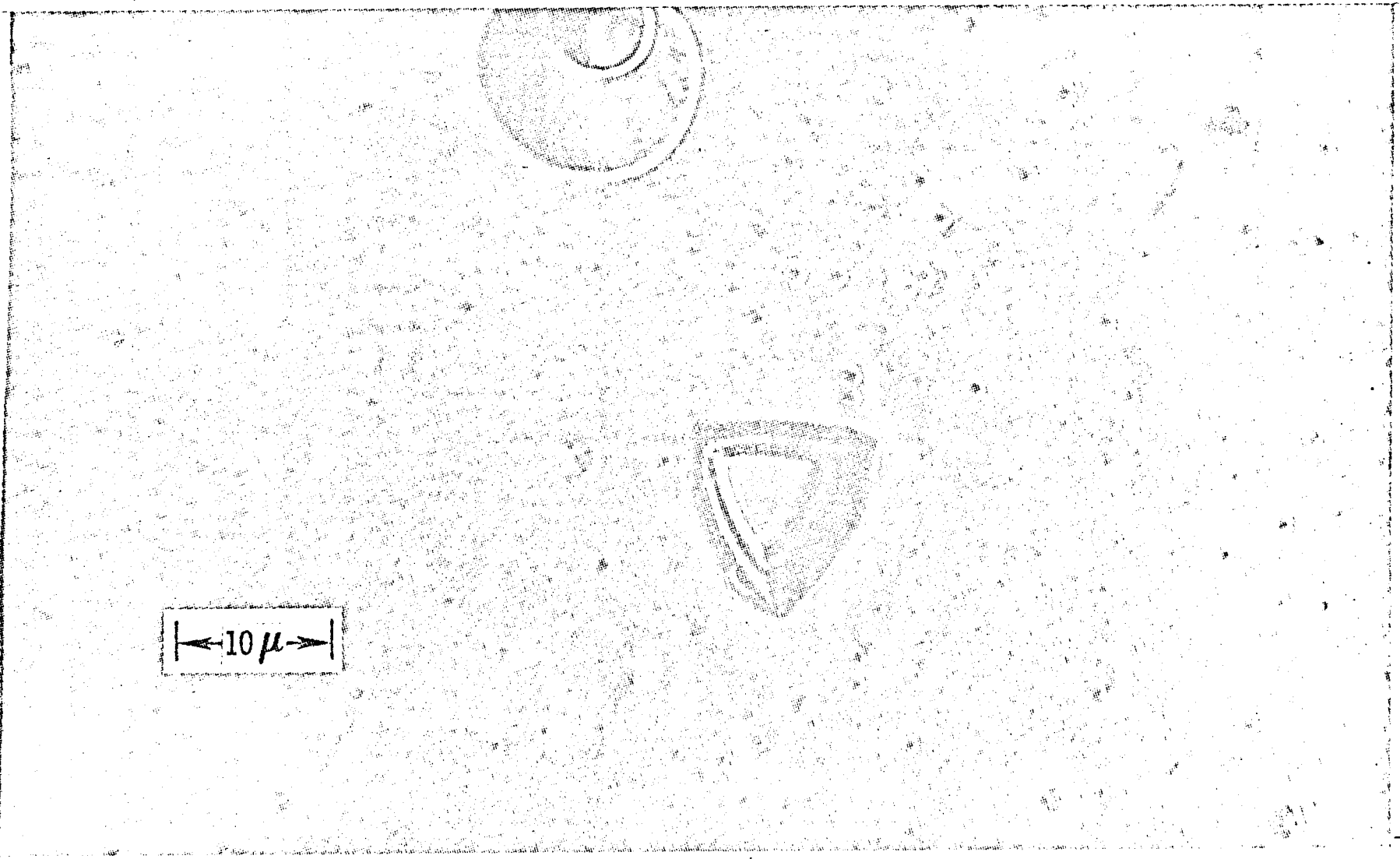

M-37726

# ETCH FIGURES ON ORTHOCLASE (001)

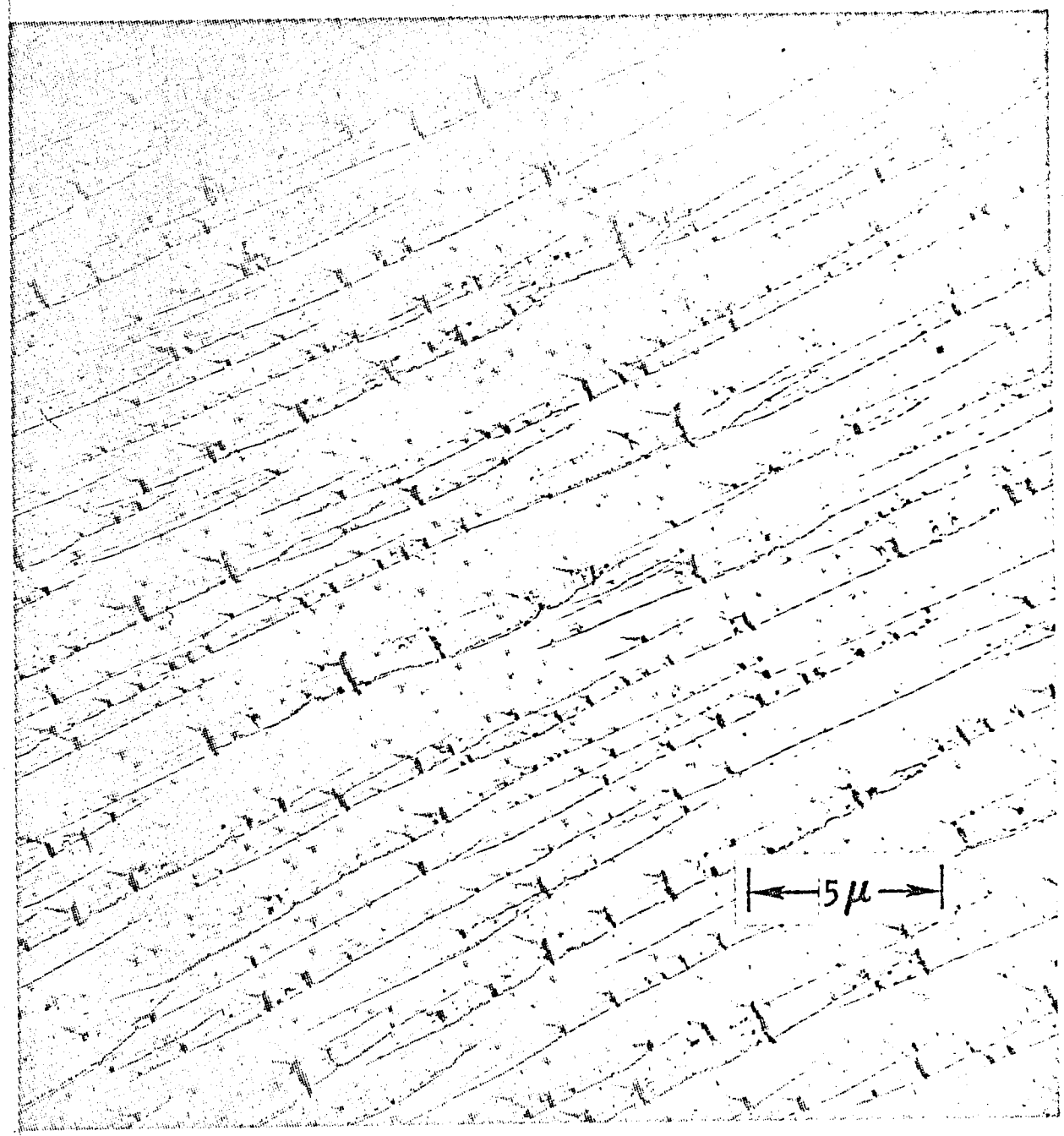

contaminated silicates, along with related studies by others, have been reported previously [3]. Hence, these results are only summarized briefly in this paper. Most emphasis is given to the results from the vacuum cleavage studies.

## Experimental

Details of the techniques of sample fabrication, cleaning and mounting, also, the experimental equipment, have been detailed elsewhere [3, 4, 5]. These are summarized briefly in this section.

### Samples and Preparation

The silicate samples chosen were, among the minerals, orthoclase, albite, bytownite, hornblende, hypersthene, labradorite, microcline, and andesine. In addition, a tektite and an obsidian were studied as representatives of disordered silicate structures. This set was chosen because the minerals are of common occurrence and represent a large range of silicate structures. Details of the chemical and physical properties of these materials are given by Dana [6].

The engineering materials chosen were aluminum (pure; 2024), alumina, titanium (6Al4V), magnesium (pure; AZ 31B), beryllium, nickel, and commercial glass (Corning #1723). These materials were chosen in part because of their possible use for lunar missions and in part because of their general interest for research purposes.

The samples for the study of adhesion between air-formed surfaces were fabricated into disks about 0.3 cm long and 0.5 cm in diameter. The samples for surface production in vacuum, by cleavage, were formed into disks of the

same diameter, but twice the length, and were notched at the point cleavage was desired.

Vacuum System and Experimental Apparatus

The vacuum system is of essentially all-metal construction (304 stainless steel). Roughing is done with a bank of three sorption pumps; the main system pump is a 200 l $sec^{-1}$ ion pump. Pressure is monitored with a "nude" Bayard-Alpert ionization gage.

The experimental apparatus used for measuring adhesion between the air-formed surfaces is shown schematically in Fig. 1. An electromagnet was used to apply load force (up to $10^6$ dynes) to the samples for the study of the dependence of adhesion on load. Loading was produced by the attraction of the metal bucket toward the magnet. The magnet current was then reduced to zero and the magnet withdrawn. Adhesion force was measured with a torsion microbalance. This balance can measure forces as small as $2 \times 10^{-2}$ dynes and as large as $4 \times 10^2$ dynes.

This system was modified for the vacuum cleavage experiments principally by the replacement of the balance with a precision mechanical spring attached to a linear motion feedthru (Fig. 2). Adhesion force was then determined by reading the spring deflection with a cathetometer. The spring allowed measurement of adhesion force as small as $10^2$ dynes and as large as $2 \times 10^4$ dynes. Cleavage was obtained by applying a gradually increasing pressure to a chisel, the tip of which was inserted into a pre-cut notch in the sample. The chisel blade was shaped so that pressure was applied only to the side faces of the slot, as shown in Fig. 2.

## Data

### Air-Formed Silicates Contacting Air-Formed Silicates

Representative data for this series of runs are given in Fig. 3. This figure shows adhesion force as a function of load force, at room temperature. It is seen that initially as load force is increased there is only a small increase in the adhesion force, but above a given load force the adhesion force begins to increase very rapidly.

System pressure for most runs was in the range 1-3 x $10^{-10}$ torr; in no case was the pressure above 6 x $10^{-10}$ torr. The sample surface roughness was in all cases between approximately 3-5 microns peak to peak.

In no case was adhesion detected prior to system evacuation. Adhesion appeared, however, once base pressure was achieved. Introduction of nitrogen to the system (to atmospheric pressure) sufficed to cause immediate disappearance of the relatively high magnitude adhesion appearing under load. However, the low load, low magnitude adhesion tended to persist until air was admitted, at which time it disappeared also.

Photomicrographic study of the contacting surfaces revealed that if the relatively large adhesion was present at vacuum, a considerable amount of surface damage and material transfer occurred. Alternatively, no surface change occurred when only low magnitude adhesion was observed.

### Air-Formed Silicates Contacting Engineering Materials

Representative data for this series of runs are shown in Fig. 4. The general experimental conditions and observations were the same as for the silicate-

silicate runs described in the previous sub-section.

Vacuum Cleaved Silicates

Some of the data obtained to date for this series of runs are presented in Figs. 5 and 6. These figures show adhesion force as a function of time after cleavage for various sample materials and orientations. The data were obtained at room temperature and no load force was applied. System pressure, at cleavage, was in all cases in the range $8 \times 10^{-11}$ to $4 \times 10^{-10}$ torr. A gas burst was noted for most runs during the period about cleavage. The gas source is not the sample itself since this behavior could be reproduced by performing all operations associated with cleavage except the cleavage itself. Rather, it appears to be due to desorption from the chamber walls caused by system vibration. The bursts, for the runs shown, did not exceed the $10^{-10}$ torr range.

It is seen that the adhesion shows a rapid initial decrease after cleavage followed generally by a long period during which little change occurs. This is particularly evident in Fig. 6. The adhesion magnitude is also much larger than that observed for the air-formed surface runs.

A rather strong long range attractive force was found to be present generally. In many instances it was sufficiently strong to pull the samples into contact for separations less than 1-2 mm. It was also capable of rotating and displacing the samples into their pre-cleavage match even with considerable initial mismatch after cleavage. The greatest such effect noted to date was one run where the force overcame a $30^{\circ}$ mismatch in rotation (upper sample with respect to the lower sample) and a 1 mm lateral displacement. Additionally, it has been found that for some runs this force caused attraction to any metal in the vicinity, whereas in other runs there was no attraction.

All indications of adhesion, and the long range force, disappeared immediately upon returning the system to atmospheric pressure.

## Discussion

### Air-Formed Surface Adhesion

Detailed discussion and interpretation of the adhesional behavior of the air-formed surfaces have been given previously [3, 4, 5]. These are summarized here primarily for comparison with the results obtained with the vacuum cleaved samples.

Two types of behavior are evident from Figs. 3 and 4. The first type, appearing at higher load, is characterized by a very rapid rise in the adhesion force as load force increases, by being present only at ultrahigh vacuum, and by producing extensive surface damage and material transfer. A particularly interesting case of the latter characteristic is shown in Fig. 7. This figure shows an essentially pure magnesium surface after contact under load with orthoclase. A number of pits and hillocks are evident. The pits represent areas where magnesium has been plucked from the surface (and deposited on the orthoclase). The hillocks appear to represent distorted areas where the forces involved were not sufficiently strong to produce a pit. Electron microprobe analysis (courtesy Dr. L. Walters, NASA Goddard) revealed that orthoclase had been deposited in the vicinity of the pits and on the tops of the hillocks. The adhesion of this orthoclase to the magnesium was quite strong, the orthoclase resisting removal by mechanical action. All observations indicate strongly that this high load adhesion is produced through the action of the silicate atomic bonding forces, and that these act only when sufficient load force is applied to cause penetration of surface contamination, and to produce sufficient distortion to permit such bonding.

The second type of adhesional behavior is characterized by its small magnitude, its presence at low load, its relative insensitivity to increase in load force, its persistence in nitrogen at atmospheric pressure, and its apparent inability to cause surface damage and material transfer. An additional observation, reported in the references given above, is that the magnitude of this adhesion increases rapidly as surface roughness decreases (in contrast to the high-load adhesion which appears to be independent of roughness). All these observations indicate strongly that the low-load adhesion is caused through the action of the dispersion forces (London-Van der Waals).

Vacuum-Formed Surface Adhesion

The most notable differences between air-formed and vacuum-formed surface adhesion are that (1) the adhesion between the vacuum-formed surfaces is much larger particularly during the early stages after cleavage, (2) these large values are produced without the application of load force, and (3) vacuum formation produces a strong long-range attractive force which was never observed for the air-formed samples.

There are three possible adhesion-producing mechanisms for the vacuum-formed surfaces. These are the action of (1) the silicate atomic bonding forces, (2) the dispersion forces, and (3) electrostatic charging (this is in contrast to the air-formed surfaces where, besides these forces, surface contamination can play a role). Of the three it can be stated with certainty that the dispersion forces make little or no contribution to the observed adhesion. This is concluded because large magnitude adhesion has appeared for runs where the surfaces produced were, inadvertantly, of extreme roughness.

Of the remaining two possibilities, it is certain that electrostatic charging is produced during surface formation. This follows indirectly, but unavoidably, from the observations of a strong long range force which could pull the samples into contact for separation up to 1-2 mm. The case for the action of the silicate atomic bonding forces, for essentially touch contact between the samples, is not so clear.

Fig. 6 shows one of the runs of particular interest. Shortly after cleavage we see that a large adhesion force was present ($8 \times 10^3$ dynes). This force decreased rapidly during the next few minutes, bottoming out at a constant force which persisted essentially unchanged for an extended period. If we extrapolate backwards in time to shortly after cleavage we see that the adhesion force apparently was then very much larger. During the period of rapid decrease we measured, by cathetometer, the distance of sample separation at which they were pulled together, finding that this remained constant. This apparent constancy of long range force contrasted to the large decrease in adhesion indicates that during this period more than one process was acting. This initial large adhesion may be due to the action of the silicate atomic bonding forces. Additional indications that this may be the case were noted for several runs, not shown, where the samples contacted surrounding system components resulting in transfer and adherence of metal to the sample. For the period following the rapid decrease, however, it appears rather definite that the surface charging is primarily, if not entirely, responsible for the adhesion.

The possible origin of this surface charging is worth note. During the initial vacuum cleavage runs we observed only a direct attraction (no

rotation or displacement) which indicated to us that the charge was probably produced through the breakage of the atomic bonds. That is, silicates possess a number of different types of atoms (ions) and when cleavage (or fracture) occurs it is hence possible that either a random or non-random separation of ions occurs. For the samples studied to date the separation should be random, and hence we made some order of magnitude calculations to determine whether the observed force could be explained on this basis. It was found that a charge excess of only $\approx 10^7$ elementary charges was required. Since $\approx 10^{13}$ bonds were broken in the cleavage, such a net charge is easily explainable on a random charge separation basis. However, later observations (sample rotation and displacement) indicated that the field is macroscopically anisotropic. This anisotropy cannot be explained on the basis of charge separation due to bond breakage. Rather, it appears that the defect structures of the crystals may be the major contributors. Possible charging mechanisms related to defect mechanisms are discussed by Grossman (this symposium).

## Implications to Moon

It was noted in the introduction that the material surfaces on the Moon could range from ultraclean to somewhat contaminated. Since the data obtained to date indicate that adhesional phenomena for silicates are highly dependent upon the surface state it can be expected that the adhesional behavior of lunar materials will be highly variable in both space and time. Also, that the precise behavior during a particular operation will depend upon the history of the surfaces involved, and upon the particular operation being performed. For instance, if we wish to determine the adhesion problems posed to a man walking across the surface we must ask: are the surface materials clean or contaminated; what is the material of his boot in contact

with the surface; how much abrasion of the boot and surface material can be expected; what is the amount, type and source locations of the gases released from and through the suit; and finally, will he just walk over the surface or will other operations be performed (such as breaking off rock samples, thereby producing fresh surfaces)? Probably the most important of these questions concerns the emission of gas from and through his suit since this may well determine the adhesion behavior encountered (oxygen is of particular importance since the surface is likely to be oxygen deficient). If, on the other hand we wish to drill into the surface we must ask ourselves the technique to be used, the drill material, and the temperatures that may be generated. Drilling falls into the general class of operations which must involve production of fresh surfaces and hence for which adhesion should pose the greatest problem.

Since adhesion phenomena depend so greatly on the particular conditions and the operations to be performed, discussion of what might occur in given instances can become rather involved. Nevertheless we can make some general statements based upon the laboratory findings:

(1) Adhesion will not in general be a major problem on the Moon nor will it be the major contributor to soil strength provided the following two conditions are met: a) all material surfaces in contact are contaminated, and b) the operations performed do not remove the contamination nor load the soil to any large degree.

If these conditions are met the adhesion will be caused primarily if not entirely by the dispersion forces and the magnitude of the adhesion, considering the grain irregularity and the surface roughness of the majority of engineering

surfaces, will be small. The only possible difficulties would involve optically flat surfaces and those used to produce vacuum (or air) tight seals. If these conditions are violated then the importance of adhesion can be expected to increase greatly. The case where clean surfaces are produced is discussed below. If the surfaces are heavily loaded the magnitude of the adhesion force can be expected to increase rapidly. For the soil itself this means that adhesion can now contribute significantly to the strength (the load it can support) and from Fig. 3 we see that the soil behavior will depend strongly upon its loading history. Additionally, the adherence of the soil to engineering materials will increase and material transfer and surface disruption will occur. This is of particular importance to critical components such as optical and thermal control surfaces and indicates that during removal of soil material deposited on these surfaces great care should be taken not to apply load force (i.e. mechanical removal techniques should be avoided if possible).

(2) Adhesion can become a major problem on the Moon and be the major contributor to soil strength if: a) the soil surfaces are ultra-clean and the engineering material surfaces are cleaned by mechanical abrasion or sputtering, or b) the operations performed produce fresh surfaces.

The magnitude of the adhesion in this case will be much larger than for the contaminated surface case and the general problems correspondingly more severe. In addition, a considerable

amount of surface electrostatic charging can be expected. This long range electrostatic force, in particular, will make it difficult to remove adhering material by mechanical means. An additional problem of note is that if the soil strength is determined primarily by adhesion, large decreases in strength can occur if the operations we perform upon the soil add contamination to the grain surfaces.

## Conclusions

The following conclusions concerning the adhesional behavior of silicates have been reached in this paper:

(1) The adhesion between contaminated surfaces is generally low and produced by the action of dispersion forces, provided the surfaces are not loaded to any great degree. The adhesion increases rapidly under load and produces material transfer and surface disruption.

(2) The adhesion between "clean" surfaces is much larger than between contaminated surfaces, and the formation of clean dielectric surfaces in vacuum produces a considerable amount of surface electrostatic charging.

(3) Since both clean and contaminated surfaces may exist now, or in the future, on the Moon, the data indicate that a large range of adhesional phenomena can be expected on the Moon.

Acknowledgement

This work is funded by the National Aeronautics and Space Administration under Contract NAS7-307.

Footnote Page

1. Chief, Lunar and Planetary Sciences Branch, Space Sciences Department, Douglas Aircraft Company, Santa Monica, California

2. Lunar and Planetary Sciences Branch, Space Sciences Department, Douglas Aircraft Company, Santa Monica, California.

3. J. A. Ryan, "Adhesion of Silicates in Ultrahigh Vacuum," J. Geophys. Res., Vol. 71, 1966, pp. 4413-4426.

4. J. A. Ryan, "Experimental Investigation of Ultrahigh Vacuum Adhesion as Related to the Lunar Surface: First Year Summary," Douglas Report SM-47914, 1965.

5. J. A. Ryan, "Experimental Investigation of Ultrahigh Vacuum Adhesion as Related to the Lunar Surface: Second Year Summary," Douglas Report DAC-59288, 1966.

6. J. D. Dana, Dana's Manual of Minerology, Sixteenth Edition, revised by C. S. Hurlbut, Jr., John Wiley & Sons, Inc., New York, 1953.

Figure 1 - - Experimental Apparatus for Studying Adhesion Between Materials Whose Surfaces were Formed in Air.

Figure 2 - - Experimental Apparatus for Performing Vacuum Cleavage and Measuring Resultant Adhesion.

Figure 3 - - Adhesion Force as a Function of Load Force for Various Silicates Whose Contact Surfaces were Formed in Air.

Figure 4 - - Adhesion Force as a Function of Load Force for Various Silicates Contacting Engineering Materials. All Contacting Surfaces were Formed in Air.

Figure 5 - - Adhesion Force as a Function of Time for Various Silicates Whose Surfaces to be Contacted were Formed at Ultrahigh Vacuum by Cleavage.

Figure 6 - - Adhesion Force as a Function of Time for Ultrahigh Vacuum Cleaved Orthoclase. The Adhesion Force is the Largest Measured to Date.

Figure 7 - - Photomicrograph of Magnesium Surface after Contact with Orthoclase at Ultrahigh Vacuum. Pits Represent Areas Where Magnesium has been Plucked from the Surface; Hillocks Represent Deformed Areas. Orthoclase has been Deposited on the Much Softer Magnesium Surface.

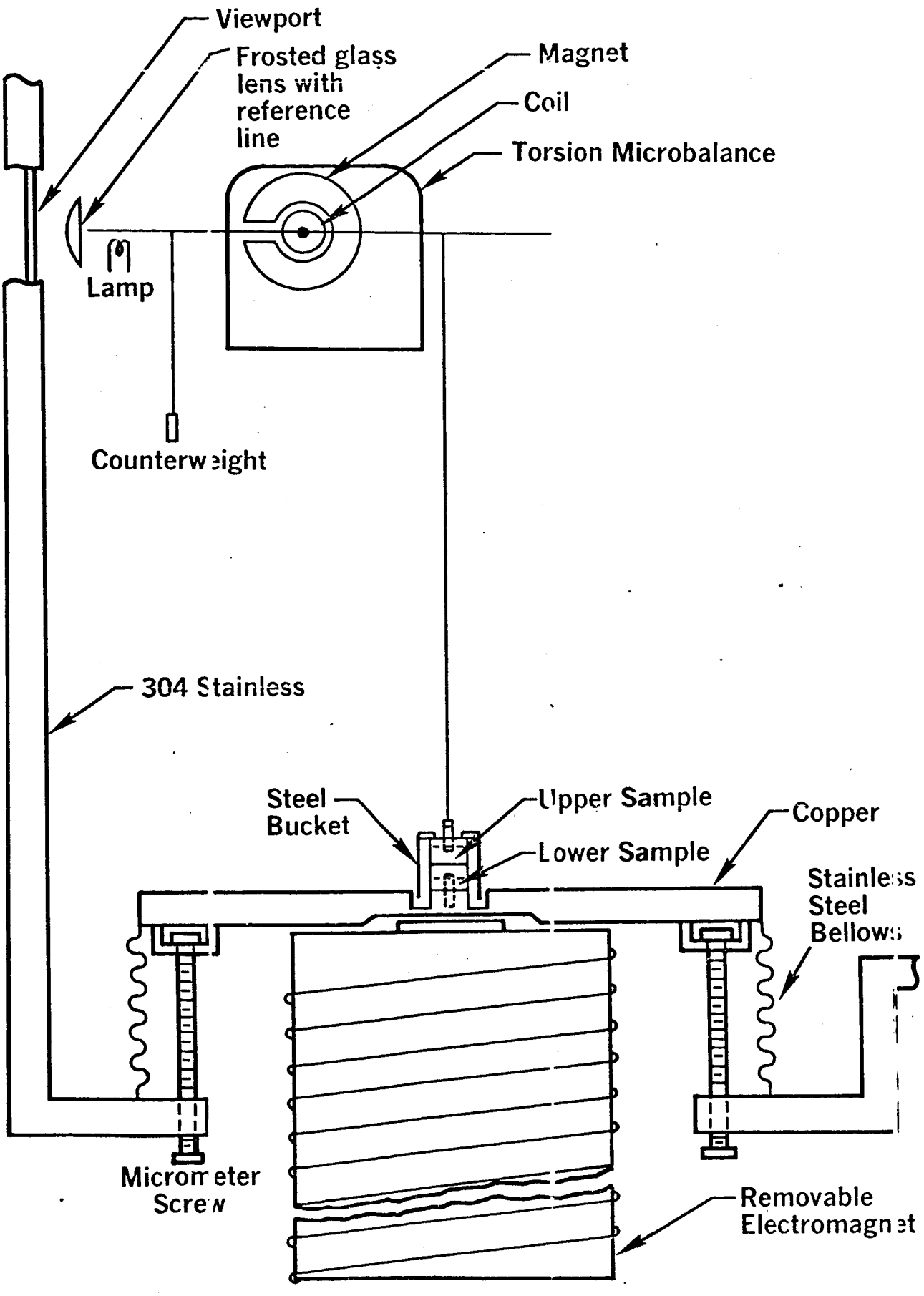
Viewport
Frosted glass lens with reference line
Magnet
Coil
Torsion Microbalance
Lamp
Counterweight
304 Stainless
Steel Bucket
Upper Sample
Lower Sample
Copper
Stainless Steel Bellows
Micrometer Screw
Removable Electromagnet

Fig. 1

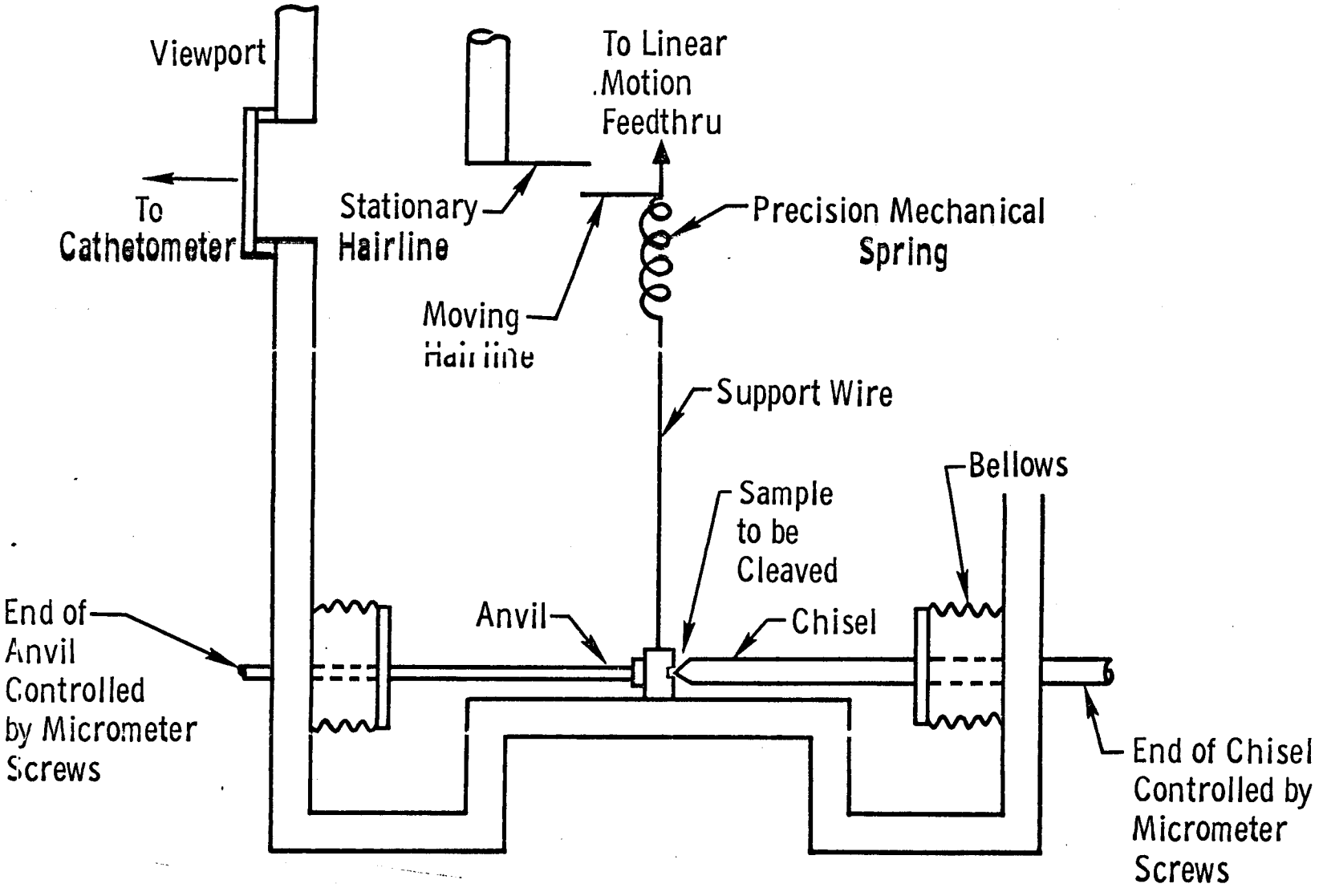
Viewport
To Linear Motion Feedthru
To Cathetometer
Stationary Hairline
Precision Mechanical Spring
Moving Hairline
Support Wire
Bellows
Sample to be Cleaved
End of Anvil Controlled by Micrometer Screws
Anvil
Chisel
End of Chisel Controlled by Micrometer Screws

Fig. 2

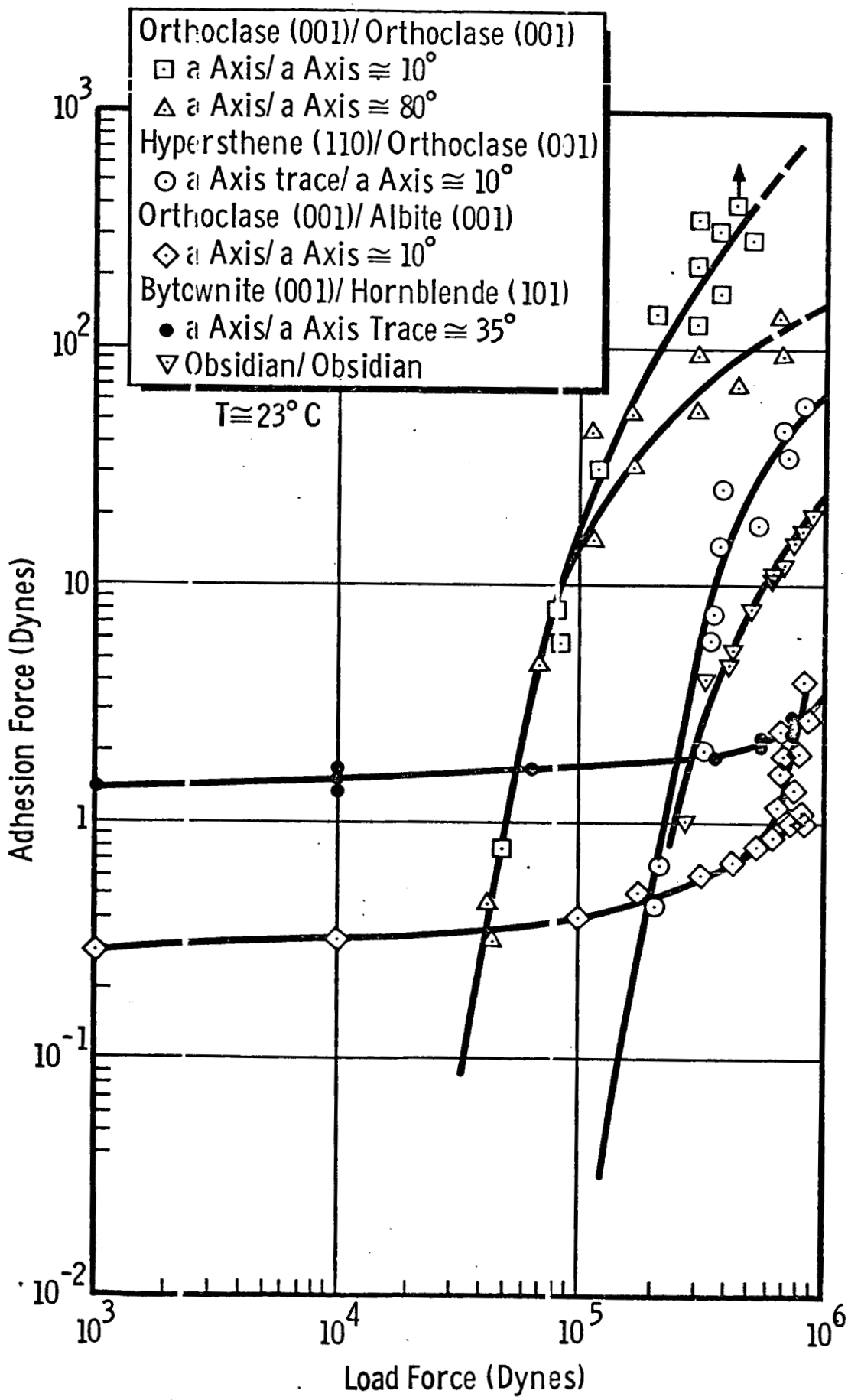
Orthoclase (001)/ Orthoclase (001)
⊡ a Axis/ a Axis ≅ 10°
△ a Axis/ a Axis ≅ 80°
Hypersthene (110)/ Orthoclase (001)
⊙ a Axis trace/ a Axis ≅ 10°
Orthoclase (001)/ Albite (001)
◇ a Axis/ a Axis ≅ 10°
Bytownite (001)/ Hornblende (101)
● a Axis/ a Axis Trace ≅ 35°
▽ Obsidian/ Obsidian
T≅23° C
Adhesion Force (Dynes)
Load Force (Dynes)
10^3
10^2
10
1
10^-1
10^-2
10^3
10^4
10^5
10^6

Fig. 3

M-37193

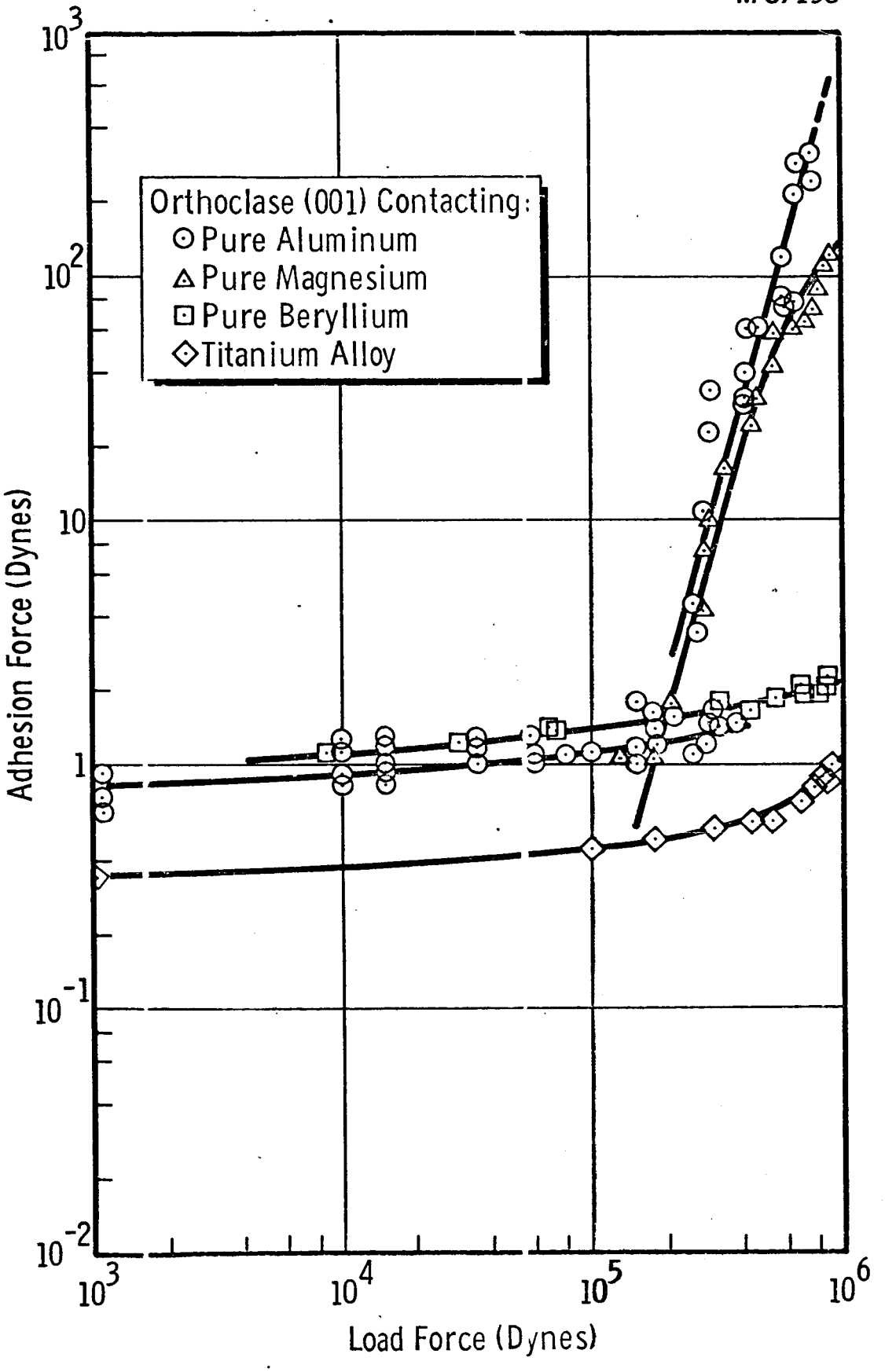
Orthoclase (001) Contacting:
Pure Aluminum
Pure Magnesium
Pure Beryllium
Titanium Alloy
Adhesion Force (Dynes)
Load Force (Dynes)
$10^3$
$10^2$
10
1
$10^{-1}$
$10^{-2}$
$10^3$
$10^4$
$10^5$
$10^6$

Fig. 4

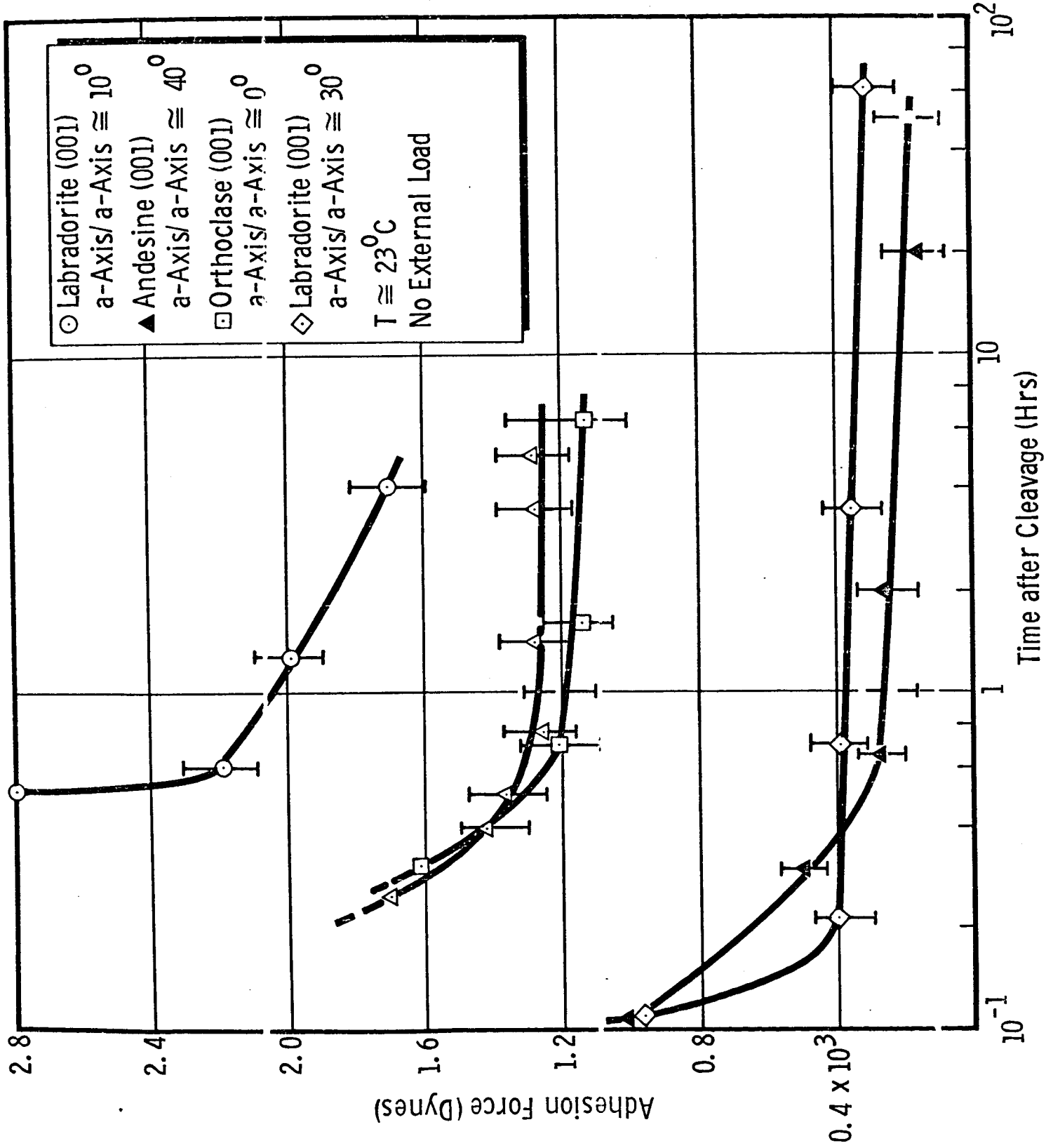
⊙ Labradorite (001) a-Axis/ a-Axis ≅ 10°
▲ Andesine (001) a-Axis/ a-Axis ≅ 40°
⊡ Orthoclase (001) a-Axis/ a-Axis ≅ 0°
◇ Labradorite (001) a-Axis/ a-Axis ≅ 30°
T ≅ 23°C
No External Load
Adhesion Force (Dynes)
Time after Cleavage (Hrs)
2.8
2.4
2.0
1.6
1.2
0.8
0.4 x 10³
10⁻¹
1
10
10²

Fig. 5

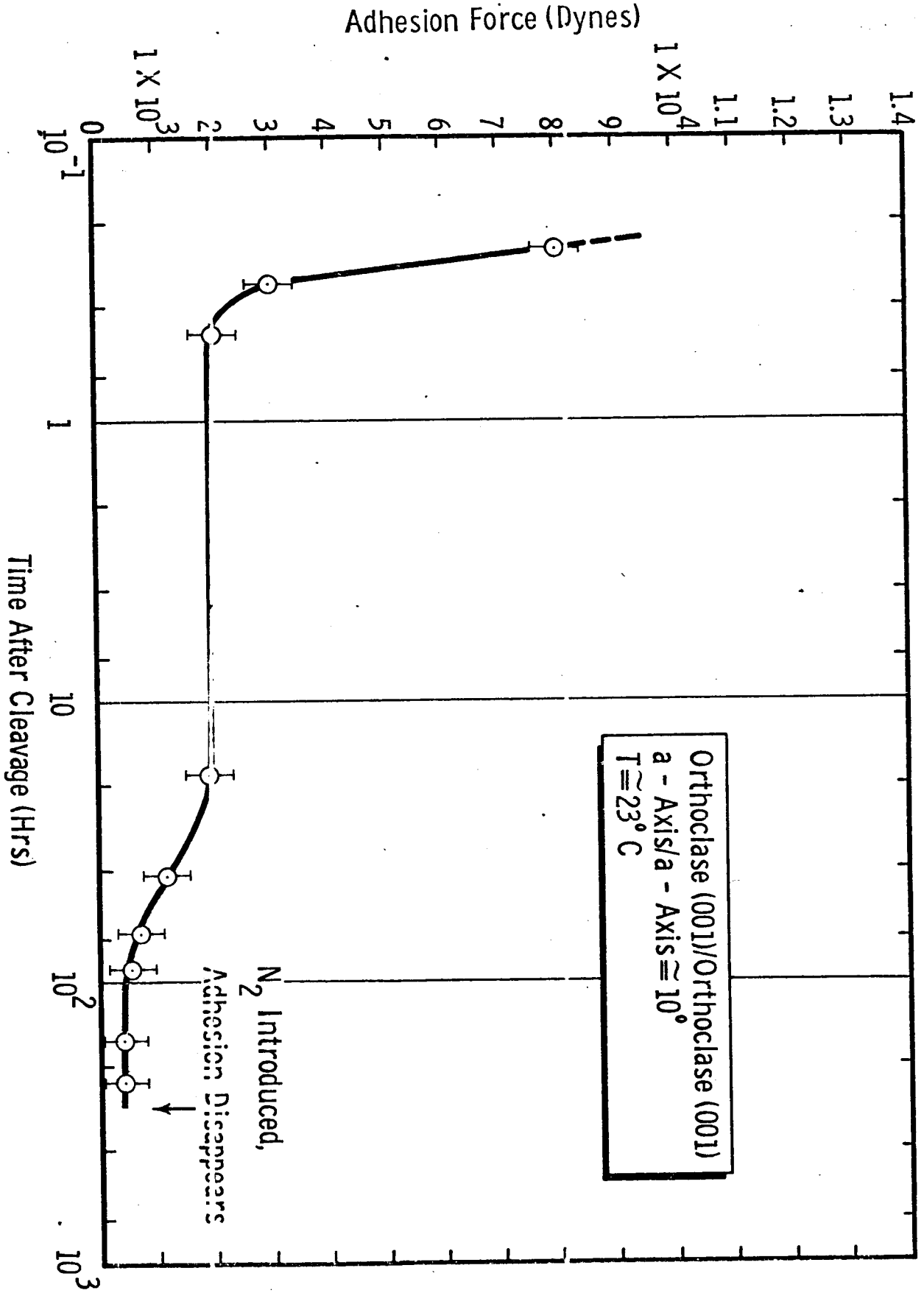
Adhesion Force (Dynes)
1 X 10^3
1 X 10^4
0
1
2
3
4
5
6
7
8
9
1.1
1.2
1.3
1.4
10^-1
1
10
10^2
10^3
Time After Cleavage (Hrs)
Orthoclase (001)/Orthoclase (001)
a - Axis/a - Axis ≅ 10°
T ≅ 23° C
N2 Introduced,
Adhesion Disappears

Fig. 6

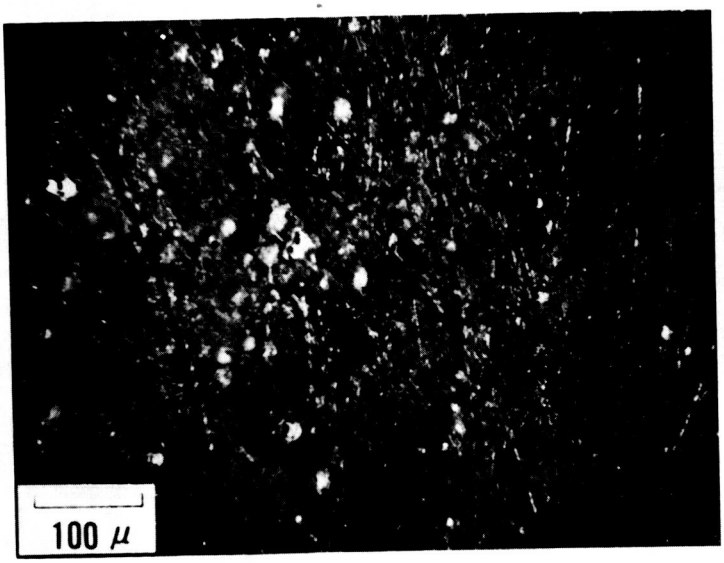


Fig. 7